Kinetics of the shear banding instability in startup flows

S. M. Fielding* and P. D. Olmsted†
Polymer IRC and Department of Physics & Astronomy, University of Leeds, Leeds LS2 9JT, United Kingdom
(Received 30 August 2002; published 30 September 2003)

Motivated by recent light scattering experiments on semidilute wormlike micelles, we study the early stages of the shear banding instability using the nonlocal Johnson-Segalman model with a ''two-fluid'' coupling of flow to micellar concentration. We perform a linear stability analysis for coupled fluctuations in shear rate $\dot{\gamma}$, micellar strain $\underline{\underline{W}}$, and concentration ϕ about an initially homogeneous state. This resembles the Cahn-Hilliard (CH) analysis of fluid-fluid demixing (although we discuss important differences). First, assuming the initial state to lie on the intrinsic constitutive curve, we calculate the ''spinodal'' onset of instability in sweeps along this curve. We then consider start-up ''quenches'' into the unstable region. Here the instability in general occurs before the intrinsic constitutive curve can be attained, so we analyze the fluctuations with respect to the *time-dependent* start-up flow. We calculate the selected length and time scales at which inhomogeneity first emerges. When the coupling between flow and concentration is switched off, fluctuations in the ''mechanical variables'' $\dot{\gamma}$ and $\underline{\underline{W}}$ are independent of those in ϕ, and are unstable when the intrinsic constitutive curve has negative slope; but no length scale is selected. Coupling to the concentration enhances this instability at short length scales, thereby selecting a length scale, consistent with the recent light scattering experiments. The spinodal region is then broadened by an extent that increases with proximity to an underlying (zero-shear) CH fluid-fluid (ϕ) demixing instability. Far from demixing, the broadening is slight and the instability is still mechanically dominated (by $\delta\dot{\gamma}$ and $\delta\underline{\underline{W}}$) with only small $\delta\phi$. Close to demixing, instability sets in at a very low shear rate, where it is dominated instead by $\delta\phi$. In this way, the model captures a smooth crossover from shear banding instabilities that are perturbed by concentration coupling to demixing instabilities that are induced by shear.

DOI: 10.1103/PhysRevE.68.036313 PACS number(s): 47.50.+d, 47.20.−k, 36.20.−r

I. INTRODUCTION

For many complex fluids, the intrinsic constitutive curve of shear stress Σ as a function of shear rate $\dot{\gamma}$ is nonmonotonic, admitting multiple values of the shear rate at a common stress. For example, Cates' model for semidilute wormlike micelles [1] predicts that the steady shear stress decreases above a critical $\dot{\gamma}=\dot{\gamma}_{c1}$ (*CE* in Fig. 1). At very high shear rates, fast relaxation processes must eventually restore an increasing stress [2,3], giving an overall curve *ACEG*. In the regime $\dot{\gamma}_{c1}<\dot{\gamma}<\dot{\gamma}_{c2}$ of decreasing stress, steady homogeneous flow [Fig. 2(a)] is unstable [4]. For an applied shear rate $\bar{\dot{\gamma}}$ in this unstable range, Spenley, Cates, and McLeish [3] predicted that the system must separate into high and low shear rate bands ($\dot{\gamma}_h$ and $\dot{\gamma}_\ell$) with relative volume fractions satisfying the applied shear rate $\bar{\dot{\gamma}}$ [Fig. 2(b)].

In any local constitutive model, the shear stress of any such banded state is not uniquely selected; it depends on initial conditions [5–9]. However, the inclusion of interfacial gradient terms into the constitutive equation turns the stress selection problem into the search for a stationary ''front'' between the low and high shear rate bands. This is satisfied only by a unique total stress $\Sigma=\Sigma_{sel}$ [6,10–12]. The steady-state flow curve then has the form *ABFG* in Fig. 1. Within the banding regime *BF* a change in the applied shear rate adjusts the relative fraction of the bands while the steady-state stress Σ_{sel} (common to both) remains constant.

Experimentally, this shear banding scenario is now well established for shear-thinning wormlike micelles [13–15]. The steady-state flow curve has a well defined, reproducible plateau Σ_{sel}. The coexistence of high and low viscosity bands has been observed by NMR spectroscopy [14,16–18]. Further evidence comes from small angle neutron scattering [13,19–23], and from flow birefringence (FB) [24–27], which reveals a (quasi)nematic birefringence band coexisting with an isotropic one. The nematic band of FB has commonly been identified with the low viscosity band of NMR; but see [28,29].

In this paper, we consider banding formation kinetics. Experimentally [13,15,30–34], in rapid upward stress sweeps the shear rate initially follows the steady-state flow curve (*AB* in Fig. 1) before departing for stresses $\Sigma>\Sigma_{sel}$ along a metastable branch (*BC*). When this branch starts to level off

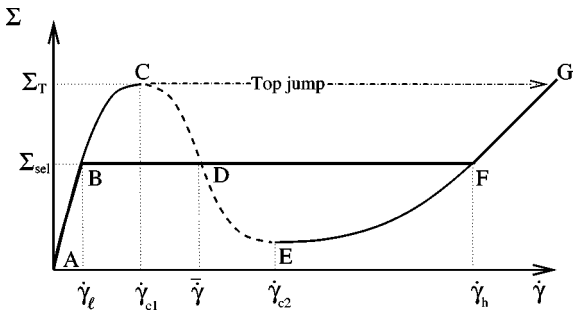

FIG. 1. Schematic flow curve for wormlike micelles.

*Electronic address: physf@irc.leeds.ac.uk
†Electronic address: p.d.olmsted@leeds.ac.uk

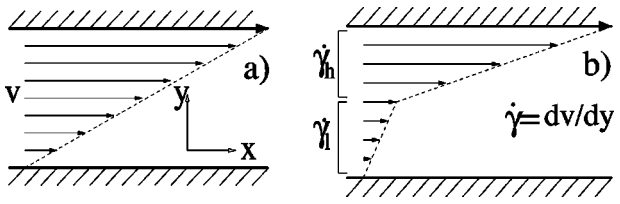

FIG. 2. (a) Homogeneous shear rate and (b) banded profiles.

(hinting of at an unstable branch for $\dot{\gamma} \gtrsim \dot{\gamma}_{c1}$) the shear rate finally ''top jumps.'' Under shear start-up (imposed $\dot{\gamma}$) in the metastable region $\dot{\gamma}_\ell < \dot{\gamma} \lesssim \dot{\gamma}_{c1}$, the stress first rapidly attains the metastable branch *BC* (sometimes via oscillations), before slowly decaying onto the steady-state plateau Σ_{sel} via a ''sigmoidal'' envelope $\exp[-(t/\tau_{NG})^\alpha]$. The time scale $\tau_{NG} = \tau_{NG}(\dot{\gamma})$ greatly exceeds the Maxwell time scale of linear rheology. In the data of Ref. [34], for example, it has an apparent divergence as $\dot{\gamma} \to \dot{\gamma}_\ell$ from above, but decreases dramatically for larger shear rates approaching the threshold of instability, $\dot{\gamma} \approx \dot{\gamma}_{c1}$. In the same experiments, the stretching exponent $\alpha \approx 2$ in the metastable regime, with a crossover to $\alpha \approx 1$ for $\dot{\gamma} \gtrsim \dot{\gamma}_{c1}$ signifying the onset of true instability.

In other systems [32], the onset of instability near $\dot{\gamma} \approx \dot{\gamma}_{c1}$ is marked (in start-up) by a huge stress overshoot that rapidly subsides to Σ_{sel} via damped oscillations. Notably, this overshoot often coincides with strongly enhanced concentration fluctuations [32], seen as butterfly patterns in light scattering with a peak amplitude at a selected length scale ~ 1 μm. This clearly suggests that flow-concentration coupling plays an important role in the shear banding instability in wormlike micelles. Further evidence comes from the slight upward slope [22] in the *steady-state* stress plateau *BF* of some systems. This is most readily explained (in planar shear at least) by a concentration difference between the coexisting bands [11,35]. Any coupling to concentration has important implications for the kinetics of macroscopic band formation, due to the large time scales involved in diffusion.

Coupling between flow and concentration is already known to be an important effect in sheared polymer solutions [36,37] and (more recently) wormlike micellar solutions [38,39] that are marginally miscible, i.e., close to an underlying fluid-fluid demixing instability. In these systems, even rather weak shear causes dramatically enhanced concentration fluctuations in steady state, interpreted as a precursor to a shear-induced demixing (SID) instability at higher shear rates. Notably, the associated butterfly patterns strikingly resemble those seen in the shear banding start-up experiments of Ref. [32], described above. In both cases, the scattering is strongest perpendicular to the compression axis of the shear, contrary to immediate intuition.

While the SID of marginally miscible polymers [36,37,42] is usually seen as a perturbation of the nearby thermodynamic demixing instability (prematurely triggered by shear), the shear banding of semidilute wormlike micelles is often attributed to a purely ''mechanical'' origin (in the unstable negatively sloping constitutive curve) [3,4]. In this work, we present a model that conceptually *unifies* these instabilities, smoothly interpolating between ''mechanical'' shear banding instabilities and SID, with increasing proximity to zero-shear demixing.

Our approach couples the nonlocal ''diffusive'' Johnson-Segalman (d-JS) model [6,40] for the dynamics of the micellar stress to a two-fluid model [41–44] for concentration fluctuations. The d-JS model is the simplest tensorial model with a flow curve of negative slope, allowing a flow instability of the type shown in Fig. 1. The two-fluid model captures the so called Helfand-Fredrickson coupling of concentration to flow [45], used previously to describe shear-enhanced concentration fluctuations, SID, and viscoelastic phase separation in marginally miscible polymer solutions with monotonically increasing stress, $d\Sigma_{xy}/d\dot{\gamma} > 0$ [36,41,45–48,48–53]. In essence, parts of a shear-extended polymer molecule (or micelle) that are in regions of lower viscosity will, during the process of relaxing to equilibrium, move more than those parts mired in a region of higher viscosity and concentration. A relaxing molecule therefore on average moves toward the higher concentration region, providing a positive feedback mechanism whereby shear can enhance concentration fluctuations and cause SID.

Within this two-fluid Johnson Segalman (d-JS-ϕ) model, we study the initial stage of instability in the unstable regime by performing a linear stability analysis [similar in spirit to the Cahn-Hilliard (CH) calculation for conventional liquid-liquid demixing] for coupled fluctuations in shear rate, micellar stress, and concentration about an initially homogeneous shear state. We calculate the ''spinodal'' boundary of the region in which these fluctuations are unstable. We then consider start-up ''quenches'' into the unstable region, predicting the selected length and time scales at which inhomogeneity first emerges (the peak amplitude of any developing scattering pattern). We also discuss the physical nature of the growing instability, according to whether its eigenvector is dominated by the flow variables or by concentration.

We introduced and briefly analyzed the d-JS-ϕ model in a previous Letter [54]. In this work we discuss more fully the model's origin and approximations and give detailed numerical and analytical arguments supporting the results announced in Ref. [54].

The paper is structured as follows. In Sec. II we introduce the model and describe its intrinsic constitutive curves. In Sec. III we review its separate shear banding and demixing instabilities when the coupling mechanism between flow and concentration is switched off. We then study the unified instability of the coupled model, performing a linear stability analysis for its initial stage. We do this in two parts. In Sec. IV we consider shear rate sweeps along the intrinsic constitutive curve, to define the spinodal onset of instability. In Sec. V we consider shear start-up ''quenches'' into the unstable region. We conclude in Sec. VI.

II. THE MODEL

The existing literature contains several approaches for coupling concentration and flow [36,41,45–49]. The two-fluid model considered by us follows closely that of Milner

[47], although we extend his work slightly by including a Newtonian contribution to the micellar stress, for reasons discussed in Sec. IV C 1. (Milner was mainly interested in slow shear phenomena, for which the Newtonian terms are unimportant.)

The basic assumption of the two-fluid model is a separate force balance for the micelles (velocity $\underline{v}_{\rm m}$) and the solvent (velocity $\underline{v}_{\rm s}$) within any element of solution. These are added to give the force balance for the center of mass velocity

$$\underline{v}=\phi\underline{v}_{\rm m}+(1-\phi)\underline{v}_{\rm s}, \tag{2.1}$$

and subtracted for the relative velocity

$$\underline{v}_{\rm rel}=\underline{v}_{\rm m}-\underline{v}_{\rm s}, \tag{2.2}$$

which in turn specifies the concentration fluctuations. We give these dynamical equations in Sec. II B below. First, we specify the free energy.

A. Free energy

In a sheared fluid, one cannot strictly define a free energy because shear drives the system out of equilibrium. Nonetheless, for realistic experimental shear rates many of the internal degrees of freedom of a polymeric solution relax very quickly compared with the rate at which they are perturbed by the externally moving constraints. Assuming that such a separation of time scales exists, one can effectively treat these fast variables as equilibrated. By integrating over them, one can define a free energy for a given fixed configuration of the slow variables. For our purposes, the relevant slow variables are the fluid momentum $\rho\underline{v}$ and micellar concentration ϕ (which are both conserved and therefore truly slow in the hydrodynamic sense), and the micellar strain $\underline{\underline{W}}$ (which is slow for all practical purposes). $\underline{\underline{W}}$ is defined as the local strain that would have to be reversed in order to relax the micellar stress:

$$\underline{\underline{W}}=\underline{\underline{E}}\cdot\underline{\underline{E}}^{T}-\underline{\underline{\delta}} \quad \text{with} \quad \delta\underline{r}'=\underline{\underline{E}}\cdot\delta\underline{r} \tag{2.3}$$

where $\delta\underline{r}'$ is the deformed vector corresponding to the undeformed vector $\delta\underline{r}$.

The resulting free energy is assumed to comprise separate kinetic, osmotic, and elastic components:

$$F=F^{\rm K}(\underline{v})+F^{\rm o}(\phi)+F^{\rm e}(\underline{\underline{W}},\phi). \tag{2.4}$$

The kinetic component is

$$F^{\rm K}(\underline{v})=\frac{1}{2}\int d^3x\,\rho\underline{v}^2. \tag{2.5}$$

The osmotic component is

$$F^{\rm o}(\phi)=\int d^3x\left[f(\phi)+\frac{g}{2}(\underline{\nabla}\phi)^2\right]$$
$$\approx\frac{1}{2}\int d^3q(1+\xi^2q^2)f''|\phi(q)|^2, \tag{2.6}$$

where f'' is the osmotic susceptibility and ξ is the equilibrium correlation length for concentration fluctuations. The elastic component is

$$F^{\rm e}(\underline{\underline{W}},\phi)=\frac{1}{2}\int d^3xG(\phi){\rm tr}[\underline{\underline{W}}-\ln(\underline{\underline{\delta}}+\underline{\underline{W}})] \tag{2.7}$$

in which $G(\phi)$ is the plateau modulus.

B. Dynamical equations

We now specify the dynamics. As noted above, the two-fluid model considers a separate force balance for the micelles and the solvent. In any fluid element, the forces and stresses on the *micelles* are assumed to be as follows.

(1) The viscoelastic stress $\underline{\underline{\sigma}}$ communicated along the micellar backbone:

$$\underline{\underline{\sigma}}=2(\underline{\underline{W}}+\underline{\underline{\delta}})\cdot\frac{\delta F}{\delta\underline{\underline{W}}}=G(\phi)\underline{\underline{W}}. \tag{2.8}$$

(2) The osmotic force $\phi\underline{\nabla}[\delta F/\delta\phi]$, which acts directly between monomers, driving conventional cooperative micellar diffusion. (Actually, because F has contributions from both $F^{\rm o}$ *and* $F^{\rm e}$, this term also contains a ''nonlinear elastic force'' $\phi\underline{\nabla}[\delta F^{\rm e}/\delta\phi]$.)

(3) A Newtonian stress $2\phi\eta_{\rm m}\underline{\underline{D}}^0_{\rm m}$, where

$$\underline{\underline{D}}^0_{\rm m}=\underline{\underline{D}}_{\rm m}-\frac{1}{3}\underline{\underline{\delta}}\,{\rm Tr}\,\underline{\underline{D}}_{\rm m} \tag{2.9}$$

and

$$\underline{\underline{D}}_{\rm m}=\frac{1}{2}[\underline{\nabla}\,\underline{v}_{\rm m}+(\underline{\nabla}\,\underline{v}_{\rm m})^T]. \tag{2.10}$$

This arises from fast micellar relaxations such as Rouse modes. We call $\eta_{\rm m}$ the ''Rouse viscosity,'' distinct from the zero shear viscosity of the *total* micellar stress.

(4) The drag force $\zeta(\phi)\underline{v}_{\rm rel}$ impeding the relative motion of micelles and solvent. Scaling theory [55] suggests $\zeta\sim 6\pi\eta\xi^{-2}$ where η is the mean viscosity $\eta=\phi\eta_{\rm m}+(1-\phi)\eta_{\rm s}$.

(5) Stress due to gradients in the hydrostatic pressure p.

The overall micellar force balance equation is thus

$$\rho_{\rm m}\phi(\partial_t+\underline{v}_{\rm m}\cdot\underline{\nabla})\underline{v}_{\rm m}=\underline{\nabla}\cdot G(\phi)\underline{\underline{W}}-\phi\underline{\nabla}\frac{\delta F(\phi)}{\delta\phi}$$
$$+2\underline{\nabla}\cdot\phi\eta_{\rm m}\underline{\underline{D}}^0_{\rm m}-\zeta(\phi)\underline{v}_{\rm rel}-\phi\underline{\nabla}p. \tag{2.11}$$

Likewise, for the solvent we have the Newtonian viscous stress, the drag force, and the hydrostatic pressure:

$$\rho_s(1-\phi)(\partial_t+\underline{v}_s\cdot\underline{\nabla})\underline{v}_s = 2\underline{\nabla}\cdot(1-\phi)\,\eta_s\underline{\underline{D}}^0_s+\zeta(\phi)\underline{v}_{rel}-(1-\phi)\underline{\nabla}p. \tag{2.12}$$

These equations contain the basic assumption of ''dynamical asymmetry,'' i.e., that the viscoelastic stress acts only on the micelles and not on the solvent. Adding them, and assuming equal mass densities $\rho_m=\rho_s=\rho$ [56], we obtain the overall force balance equation for the center of mass motion

$$\rho(\partial_t+\underline{v}\cdot\underline{\nabla})\underline{v}-\rho\underline{v}_{rel}\underline{v}\cdot\underline{\nabla}\phi+\rho\phi(1-\phi)\underline{v}_{rel}\cdot\underline{\nabla}\underline{v}_{rel} = \underline{\nabla}\cdot G(\phi)\underline{\underline{W}}-\phi\underline{\nabla}\frac{\delta F(\phi)}{\delta\phi}+2\underline{\nabla}\cdot\phi\,\eta_m\underline{\underline{D}}^0_m + 2\underline{\nabla}\cdot(1-\phi)\,\eta_s\underline{\underline{D}}^0_s-\underline{\nabla}p, \tag{2.13}$$

in which the equal and opposite drag forces have canceled each other. The pressure p is fixed by incompressibility,

$$\underline{\nabla}\cdot\underline{v}=0. \tag{2.14}$$

We attach a cautionary note to Eq. (2.13). The right-hand side (RHS) is the net force acting on any fluid element. The LHS, therefore, should equal the rate of change of that element's momentum, $\rho(\partial_t+\underline{v}\cdot\underline{\nabla})\underline{v}$. Although this term is indeed present, we also find two extra terms, containing $\underline{v}_{rel}$. To circumvent this discrepancy, one might argue that the separate advected derivatives on the LHS's of Eqs. (2.11) and (2.12) [which were added to give Eq. (2.13)] should have $\underline{v}\cdot\underline{\nabla}\underline{v}_i$ in place of $\underline{v}_i\cdot\underline{\nabla}\underline{v}_i$ (for $i\in$ m,s). However, this would still leave the correction $-\underline{v}_{rel}\underline{v}\cdot\underline{\nabla}\phi$ on the LHS of Eq. (2.13) and does not improve the approximation. We consider this discrepancy to be an unsatisfactory aspect of the two-fluid model that is seldom acknowledged in the literature. In this paper, however, we consider only small fluctuations about a homogeneous shear state (in which $\underline{v}_{rel}=\underline{0}$), and the correction terms are truly negligible.

Subtracting the micellar and solvent Eqs. (2.11) and (2.12) (with each predivided by its own volume fraction), and neglecting small inertial terms [57] we find an expression for the relative motion:

$$\underline{v}_{rel}=\frac{\phi(1-\phi)}{\zeta(\phi)}\left[-\underline{\nabla}\frac{\delta F}{\delta\phi}+\frac{1}{\phi}\,\underline{\nabla}\cdot G(\phi)\underline{\underline{W}}+\frac{2\underline{\nabla}\cdot\phi\,\eta_m\underline{\underline{D}}^0_m}{\phi} - \frac{2\underline{\nabla}\cdot(1-\phi)\,\eta_s\underline{\underline{D}}^0_s}{1-\phi}\right], \tag{2.15}$$

which in turn specifies the dynamics of the concentration fluctuations:

$$(\partial_t+\underline{v}\cdot\underline{\nabla})\phi=-\underline{\nabla}\cdot\phi(1-\phi)\underline{v}_{rel} = -\underline{\nabla}\cdot\frac{\phi^2(1-\phi)^2}{\zeta(\phi)}\left[-\underline{\nabla}\frac{\delta F}{\delta\phi}+\frac{1}{\phi}\,\underline{\nabla}\cdot G(\phi)\underline{\underline{W}} + \frac{2\underline{\nabla}\cdot\phi\,\eta_m\underline{\underline{D}}^0_m}{\phi}-\frac{2\underline{\nabla}\cdot(1-\phi)\,\eta_s\underline{\underline{D}}^0_s}{1-\phi}\right]. \tag{2.16}$$

The essence of the two-fluid model is that the viscoelastic stress $G(\phi)\underline{\underline{W}}$ appears alongside the familiar osmotic stress $-\phi\underline{\nabla}\delta F/\delta\phi$ in this diffusion equation. This causes micelles to diffuse up gradients in this stress $G(\phi)\underline{\underline{W}}$ and so couples flow to concentration [45]. If the viscoelastic stress then increases with concentration ($dG/d\phi>0$, assumed here), positive feedback occurs, causing net diffusion of micelles *up* their own concentration gradient. Although obviously opposed by the restoring osmotic force, which drives conventional micellar diffusion, this mechanism causes shear-enhanced concentration fluctuations or SID in systems already close to demixing [41,48]. In SB systems, it causes concentration coupling (see below and Refs. [54,58,59]). The overall rate of micellar diffusion is set by the kinetic drag coefficient $\zeta(\phi)$. The ''raw'' micellar diffusion coefficient in the absence of flow-concentration coupling is $D\propto f''/\zeta(\phi)$.

For the dynamics of the viscoelastic micellar backbone strain we use the phenomenological d-JS model [6,40]:

$$(\partial_t+\underline{v}_m\cdot\underline{\nabla})\underline{\underline{W}}=a(\underline{\underline{D}}_m\cdot\underline{\underline{W}}+\underline{\underline{W}}\cdot\underline{\underline{D}}_m)+(\underline{\underline{W}}\cdot\underline{\underline{\Omega}}_m-\underline{\underline{\Omega}}_m\cdot\underline{\underline{W}}) + 2\underline{\underline{D}}_m-\frac{\underline{\underline{W}}}{\tau(\phi)}+\frac{l^2}{\tau(\phi)}\,\underline{\nabla}^2\underline{\underline{W}}. \tag{2.17}$$

The terms in $\underline{v}_m$, $\underline{\underline{D}}_m$, and $\underline{\underline{\Omega}}_m$ describe convection, stretching, and rotation of the micellar strain by flow; $2\underline{\underline{\Omega}}_m=\underline{\nabla}\underline{v}_m-(\underline{\nabla}\underline{v}_m)^T$ with $(\underline{\nabla}\underline{v}_m)_{\alpha\beta}\equiv\partial_\alpha(v_m)_\beta$. The slip parameter a measures the nonaffinity of the molecular deformation, i.e., the fractional stretch of the polymeric material with respect to that of the flow field. For $|a|<1$ (slip) the intrinsic constitutive curve in planar shear is capable of the nonmonotonicity of Fig. 1, thereby admitting a shear banding instability [40]. The term $\underline{\underline{W}}/\tau$ describes relaxation of the micelles back to their unstrained state with a Maxwell time $\tau(\phi)$. The gradient term $[l^2/\tau(\phi)]\nabla^2\underline{\underline{W}}$ allows a selected banding stress to be calculated. (See Refs. [6,58], although other treatments [60,61] have used alternative forms for nonlocal terms that can also give a uniquely selected stress.) The length l could, for example, be set by the mesh size or by the equilibrium correlation length for concentration fluctuations. Here we assume the former, since the dynamics of the micellar conformation are more likely to depend on gradients in conformation than in concentration. The equilibrium correlation length ξ of course still enters our analysis, through the osmotic free energy of Eq. (2.6). Together, l and ξ set the length scale of any interfaces. We use Eqs. (2.13), (2.14), (2.16), and (2.17) as our model for the remainder of the paper.

C. Flow geometry and boundary conditions

We consider a state $\underline{\overline{v}}(y)$ of idealized homogeneous planar shear bounded by infinite plates at $y=\{0,L\}$ with $(\underline{\overline{v}}=\overline{\dot{\gamma}}y\hat{\underline{x}},\nabla\overline{v},\nabla\wedge\underline{\overline{v}})$ in the $(\hat{\underline{x}},\hat{\underline{y}},\hat{\underline{z}})$ directions. In what follows, we will analyze the stability of small fluctuations about this state, for simplicity considering fluctuation wave vectors only in the flow gradient direction, $\underline{v}=\underline{\overline{v}}(y)+\delta\underline{v}(y)$ and (separately) the vorticity direction, $\underline{v}=\underline{\overline{v}}(y)+\delta\underline{v}(z)$.

We assume that there is no slip at the plates, so for controlled average shear rate conditions (assumed throughout)

$$\overline{\dot{\gamma}}=\int_0^L dy\,\dot{\gamma}(y,z)=\text{const}\ \forall\ z. \tag{2.18}$$

In this equation, $\overline{\dot{\gamma}}$ is the applied shear rate, and

$$\dot{\gamma}(y,z)=\partial_y v_x(y,z) \tag{2.19}$$

is the local shear rate (dependent on either y or z, according to the wave vector's direction). We also assume boundary conditions [62]

$$\partial_y\phi=\partial_y^3\phi=0 \quad \text{at}\ \ y=0,L \tag{2.20}$$

and, following [6],

$$\partial_y W_{\alpha\beta}=0 \quad \forall\ \ \alpha,\beta \quad \text{at}\ \ y=0,L. \tag{2.21}$$

D. Model parameters

Typical values for the model parameters are taken as follows. We assume the solvent viscosity η_s and density ρ to be those of water. We take the plateau modulus G and the Maxwell time τ from linear rheology [63] at $\phi=0.11$ on cetyltrimethylammonium bromide (CTAB) $(0.3M)/NaNO_3(1.79M)/H_2O$. We estimate the Rouse viscosity η_m from the (limited data on the) high shear branch of the flow curve of a closely related system [63]. The mesh size is estimated to be $l\approx(k_BT/G)^{1/3}$ [55]. In fact this form is truly valid only for a good solvent, although in the interests of simplicity we assume it to be a good approximation even for systems closer to demixing. We take the diffusion coefficient D and the equilibrium correlation length ξ from dynamic light scattering (DLS) data [64] on CTAB/KBr/H_2O, at a comparable micellar volume fraction. We calculate the drag coefficient $\zeta=6\pi\eta\xi^{-2}$ [55]. We fix the slip parameter $a=0.92$ by comparing our intrinsic constitutive curve in the semidilute regime to that of Cates' model for wormlike micelles [1]. We then have realistic values for all parameters, at $\phi=0.11$ (Table I).

After a rescaling of stress, time, and length so that $G(\phi=0.11)=1$, $\tau(\phi=0.11)=1$, and $L=1$, where L is the rheometer gap (0.15 mm) used in Ref. [63], the model has eight scaled parameters. Exploring this large parameter space is a daunting prospect so we shall not, in general, vary the parameters independently. Indeed, any given spinodal is generated by simply tuning the single parameter ϕ, relying on known semidilute scaling laws for the dependence of the other parameters upon ϕ (column 4 of Table I). We do, however, calculate the spinodal for several different values of the diffusion coefficient D to investigate the effect of increasing proximity to a zero-shear demixing instability. For simplicity we assume that the slip parameter a is independent of ϕ. η_m and η_s are also assumed independent of ϕ, but are prefactored by the extensive factors ϕ and $1-\phi$, respectively, in Eqs. (2.13) and (2.16). We often eliminate ρ in favor of the Reynolds time $\tau_R=\rho L^2/\eta_s=O(10^{-3}\tau(\phi=0.11))$.

TABLE I. Experimental values of the model's parameters at volume fraction $\phi=0.11$ (column 3). Scaling laws for the dependence of each parameter upon ϕ (column 4). In most calculations we use the reference values of column 3 at $\phi=0.11$, then tune ϕ using the scaling laws of column 4. Only where stated do we allow the parameters to vary independently.

Parameter	Symbol Q	Value at $\phi=0.11$	$\frac{d\ln Q}{d\ln\phi}$
Rheometer gap	L	0.15 mm	0
Maxwell time	τ	0.17 s	1.1
Plateau modulus	G	232 Pa	2.2
Density	ρ	10^3 kg m^{-3}	0
Solvent viscosity	η_s	10^{-3} kg m^{-1} s^{-1}	0
Rouse viscosity	η_m	0.4 kg m^{-1} s^{-1}	0
Mesh size	l	2.6×10^{-8} m	-0.73
Diffusion coefficient	D	3.5×10^{-11} m^2 s^{-1}	0.77
Drag coefficient	ζ	2.4×10^{12} kg m^{-3} s^{-1}	1.54
Correlation length	ξ	6.0×10^{-7} m	-0.77
Slip parameter	a	0.92	0

E. Intrinsic constitutive curves

In planar homogeneous flow with uniform concentration $\overline{\phi}$ and shear $\overline{\dot{\gamma}}$ (with $\underline{v}_m=\underline{v}_s=\underline{v}$), the components of the micellar strain are given by

$$\overline{W}_{xy}=\frac{\overline{\dot{\gamma}}\tau(\overline{\phi})}{1+b\overline{\dot{\gamma}}^2\tau^2(\overline{\phi})},$$

$$\overline{W}_{yy}=-\frac{1}{(1+a)}\frac{b\overline{\dot{\gamma}}^2\tau^2(\overline{\phi})}{1+b\overline{\dot{\gamma}}^2\tau^2(\overline{\phi})},$$

$$\overline{W}_{xx}=\frac{1+a}{a-1}\overline{W}_{yy},$$

$$\overline{W}_{zz}=\overline{W}_{xz}=\overline{W}_{yz}=0, \tag{2.22}$$

in which

$$b=1-a^2. \tag{2.23}$$

The total shear stress is the sum of the micellar stress and a Newtonian component:

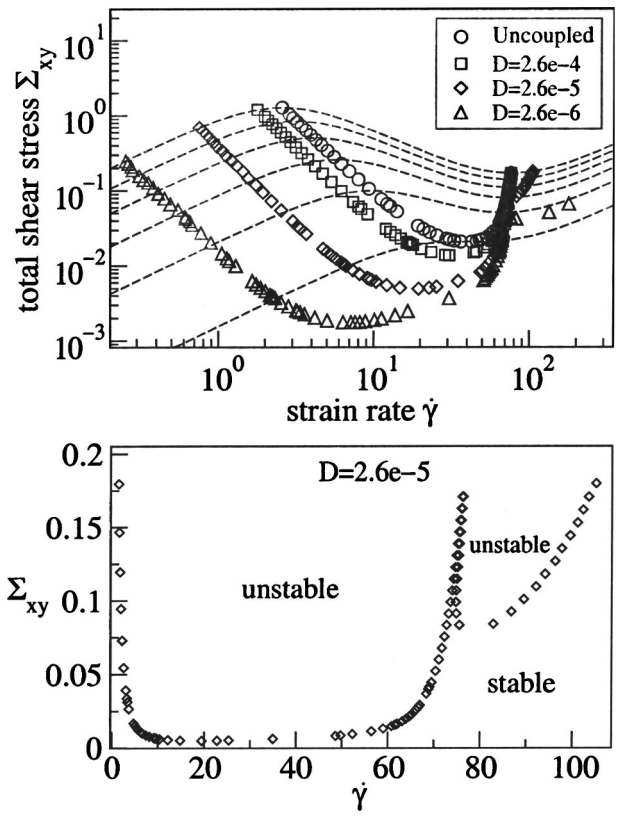

FIG. 3. Top graph: intrinsic constitutive curves for $\phi=0.11$, 0.091, 0.072, 0.053, 0.034, 0.015 (dashed lines, downward). Spinodals for the uncoupled limit $\zeta\to\infty$ ($\bigcirc$); coupled model with $D(\phi=0.11)$ taken from the DLS data (Table I) ($\square$); coupled model with D artificially reduced ($\diamond$,$\triangle$). Bottom graph: spinodal for $D=2.6\times10^{-5}$, replotted on a linear scale to show the lobe of instability at high shear rate more clearly.

$$\overline{\Sigma}(\overline{\dot{\gamma}},\overline{\phi})=G(\overline{\phi})W_{xy}(\overline{\dot{\gamma}},\overline{\phi})+\eta(\overline{\phi})\overline{\dot{\gamma}}. \tag{2.24}$$

This defines a set of intrinsic constitutive curves $\overline{\Sigma}(\overline{\dot{\gamma}},\overline{\phi})$ (dashed lines in Fig. 3), one for each concentration $\overline{\phi}$. The criterion for the nonmonotonicity of $\overline{W}_{xy}$ to dominate the Newtonian term $\eta(\overline{\phi})\overline{\dot{\gamma}}$ and cause nonmonotonicity in the overall stress $\overline{\Sigma}$ is $\eta(\overline{\phi})<\frac{1}{8}G(\overline{\phi})\tau(\overline{\phi})$. As $\overline{\phi}$ is reduced, therefore, the region of negative slope narrows, terminating in a ''critical'' point at $\overline{\phi}=\overline{\phi}_c\approx0.015$. The same qualitative trend has been seen in cetylpyridrimum chloride (CPCl) sodium salicylade (NaSal)/brine [13].

Although these intrinsic constitutive curves are *stationary* solutions, $\partial_t\cdots=0$, they are not necessarily *stable* against perturbations that can lead to shear banding and/or demixing. We now proceed to discuss the instabilities that can arise.

III. UNCOUPLED LIMIT

In the limit of infinite drag, i.e., $\zeta\to\infty$ at fixed $f''(\phi)$, the relative motion between micelles and solvent is switched off, disabling concentration fluctuations. In the slightly different limit of $\zeta\to\infty$ at fixed micellar diffusion coefficient

$$D=\frac{\phi^2(1-\phi)^2f''}{\zeta}, \tag{3.1}$$

the concentration still fluctuates, but independently of the rheological variables. Equation (2.16) then reduces to the CH equation (with a ϕ-dependent mobility). Independently of $\delta\phi$, the shear rate and micellar stress together obey uniform-ϕ d-JS dynamics [6,65,66]. Accordingly (as described in detail in Sec. IV B below), two separate instabilities are possible.

(a) Demixing instability. For $D<0$, the concentration has its own CH demixing instability, governed primarily by the free energy defined in Eq. (2.6). As noted, this occurs regardless of shear. In this work we consider only *flow-induced* instabilities, and so set $D>0$.

(b) Mechanical instability. For shear rates where the intrinsic constitutive curve has negative slope $d\Sigma/d\dot{\gamma}<0$, fluctuations in the shear rate and micellar stress have their own shear banding instability, which for convenience we call ''mechanical.''

For finite drag, these instabilities are mixed by feedback between flow and concentration. Although we always consider systems stable against zero-shear fluid-fluid demixing, $D>0$, the mechanical instability is nonetheless enhanced by coupling to concentration and can now set in at a shear rate $\dot{\gamma}<\dot{\gamma}_{c1}$, for which $d\Sigma/d\dot{\gamma}>0$. Indeed, for systems close to demixing, $D\gtrsim0$, instability sets in at $\dot{\gamma}\gtrsim0$, for which the region of negative constitutive slope for $\dot{\gamma}>\dot{\gamma}_{c1}$ is essentially irrelevant. In this way, the coupling mechanism allows a smooth crossover between ''mechanical instabilities'' (triggered mainly by the negative constitutive slope) to ''demixing, triggered by flow'' with increasing proximity to zero-shear demixing, $D=0$.

In what follows, we study in detail the onset of this combined instability. We consider two different flow histories. The first (Sec. IV) assumes an initial state on the intrinsic constitutive curve and is used to define the ''spinodal'' limit of stability in sweeps along this curve. This is analogous to defining the spinodal of a van der Waals fluid via quasistatic compression and suffers from the same practical ambiguity that *finite* fluctuations can cause separation or banding via *metastable* kinetics before the spinodal is reached. The second history (Sec. V) considers a start-up ''quench'' into the unstable region and is (essentially) the counterpart of a temperature quench into the demixing regime of a van der Waals fluid. The analysis here is complicated by the fact that the fluctuations emerge against the time-dependent start-up flow.

IV. INITIAL STATE ON INTRINSIC CONSTITUTIVE CURVE; SLOW SHEAR RATE SWEEPS

A. Linear analysis

Armed with the intuition of the previous section, we now turn to the analysis proper. In this section, we study the linear stability of homogeneous initial states on the intrinsic constitutive curve to find the spinodal onset of instability in shear rate sweeps along this curve.

Looking back at Eqs. (2.13), (2.14), (2.16), and (2.17), we recall that the model has the following dynamical order parameters: fluid velocity $\underline{v}$, local micellar strain $\underline{\underline{W}}$, and concentration ϕ. (For large drag, $\underline{v}_{\rm rel}$ is assumed to respond adiabatically.) In what follows, we will work in terms of the shear rate $\underline{\nabla}\,\underline{v}$ instead of velocity $\underline{v}$, taking the gradient of the (linearized version of the) force balance equation Eq. (2.13).

An initial homogeneous shear state on the intrinsic constitutive curve has uniform $\underline{\nabla}\,\underline{v}=\dot{\overline{\gamma}}\hat{x}\hat{y}$ and $\phi=\overline{\phi}$, with the components of $\underline{\underline{W}}(\dot{\overline{\gamma}},\overline{\phi})$ (also uniform) given by Eq. (2.22). We encode this state as follows:

$$\underline{\overline{u}}=\dot{\overline{\gamma}}\hat{\underline{e}}_{\underline{\nabla}\,\underline{v}_{xy}}+\sum_{ij}\overline{W}_{ij}\hat{\underline{e}}_{\underline{W}_{ij}}+\overline{\phi}\hat{\underline{e}}_{\phi}, \tag{4.1}$$

in which the $\hat{\underline{e}}$ are dimensionless unit vectors [67].

Noise induces fluctuations about this state, giving

$$\underline{u}(\underline{r},t)=\underline{\overline{u}}+\sum_{\underline{k}}\delta\underline{u}_{\underline{k}}(t)\exp(i\underline{k}\cdot\underline{r}), \tag{4.2}$$

with the sum covering both positive and negative $\underline{k}$, and $\delta\underline{u}_{-\underline{k}}=\delta\underline{u}_{\underline{k}}^{*}$ ensuring that $\underline{u}(\underline{r},t)$ is real. For simplicity, following numerous previous authors [4,35,48,69], we consider only fluctuation wave vectors in the velocity gradient direction $\underline{k}=k\hat{y}$ and (separately) the vorticity direction $\underline{k}=k\hat{z}$. We discard any component in the flow direction $\hat{x}$, which would be advected by the background flow, greatly complicating the analysis. Indeed, the spinodal is commonly *defined* using only these advection-free fluctuations [68]. We defer to a future paper [70] a full numerical calculation of the scattering structure factors in the entire k_x-k_y and k_x-k_z planes, as could be investigated experimentally by light scattering.

Substituting Eq. (4.2) into Eqs. (2.13), (2.14), (2.16), and (2.17) and retaining only terms linear in the fluctuations, we get an equation of the form

$$\partial_t\delta\underline{u}_{\underline{k}}(t)=\underline{\underline{M}}_{\underline{k}}\cdot\delta\underline{u}_{\underline{k}}(t)+\underline{\eta}_{\underline{k}}(t), \tag{4.3}$$

where we have now included a noise source of the fluctuations, $\underline{\eta}_{\underline{k}}(t)$. This linearized equation is valid only as long as the fluctuations remain small, and so can predict only the initial stages of fluctuation growth in any instability, which is our aim.

The stability matrix $\underline{\underline{M}}_{\underline{k}}$ determines the fate of the fluctuations. Its eigenmodes obey

$$\omega_{\underline{k},\alpha}\underline{\mathsf{v}}_{\underline{k},\alpha}=\underline{\underline{M}}_{\underline{k}}\underline{\mathsf{v}}_{\underline{k},\alpha}, \tag{4.4}$$

where α is the mode index. The eigenvalues $\omega_{\underline{k},\alpha}$ versus $\underline{k}$ define a multibranched dispersion relation. For the initial state $\underline{\overline{u}}$ to be stable (decaying fluctuations), the real part of all dispersion branches must be negative. A positive eigenvalue $\omega_{\underline{k},\alpha}$ indicates an unstable mode that grows exponentially in time with relative order-parameter amplitudes specified by the corresponding eigenvector $\underline{\mathsf{v}}_{\underline{k},\alpha}$. As the background homogeneous shear state $\underline{\overline{u}}=[\dot{\overline{\gamma}},\underline{\underline{\overline{W}}},\overline{\phi}]$ is tracked upwards (downwards) sweep along the intrinsic constitutive curve, therefore, the lower (upper) spinodal lies where the eigenvalue $\omega_{\underline{k}*}$ of $\underline{\underline{M}}_{\underline{k}}=\underline{\underline{M}}_{\underline{k}}(\underline{\overline{u}})$ with the largest real part (maximized over $\underline{k}$ and α) crosses the imaginary axis in the positive direction.

For any shear rate between the spinodals, the dispersion relation is positive for some range of wave vectors. Typically, we find just one unstable branch $\omega_{\underline{k}}$. We give results for this branch below, focusing on any global maximum, which indicates a selected length scale $\underline{k}^{*-1}$ at which inhomogeneity emerges most quickly. We also study the unstable eigenvector $\underline{\mathsf{v}}_{\underline{k}*}$ at this maximum, which encodes the ''nature'' of the instability (mechanical versus demixing).

We devote most of our attention to flow gradient fluctuations $\underline{k}=k\hat{y}$, returning at the end of this section to briefly analyze vorticity fluctuations, the stability of which turns out to be unaffected by shear in our model.

For flow gradient fluctuations, then, $\delta v_y=0$ by incompressibility and the relevant remaining components of $\delta\underline{u}_{\underline{k}}(t)$ are $ik\delta v_x=\delta\dot{\gamma},ik\delta v_z,\delta W_{xy},\delta W_{xx},\delta W_{yy},\delta W_{xz},\delta W_{yz},\delta W_{zz}$, and $\delta\phi$. Evaluating the components of the stability matrix $\underline{\underline{M}}_{\underline{k}}(\underline{\overline{u}})$, we find that it decomposes into three independent subspaces: $\mathfrak{S}_1\equiv[ik\delta v_x=\delta\dot{\gamma},\delta W_{xy},\delta W_{xx},\delta W_{yy},\delta\phi]$, $\mathfrak{S}_2=[ik\delta v_z,W_{xz},W_{yz}]$, and $\mathfrak{S}_3=W_{zz}$. In all unstable regimes, for this flow history, only $\mathfrak{S}_1$ is unstable [71], so we focus on this subspace hereafter.

While most of the results given below will be numerical, in some regimes we also give *qualitative* analytical results, obtained from the following simplified form of the relevant stability matrix in the subspace $[\delta\dot{\gamma},\ \delta W_{xy},\ \delta Z,\delta\phi]$:

$$\underline{\underline{M}}_{\underline{k}}=\begin{pmatrix}-\dfrac{\eta k^2}{\eta_s\tau_d} & -\dfrac{k^2}{\eta_s\tau_d} & 0 & -\dfrac{G'\overline{W}_{xy}k^2}{\eta_s\tau_d}\\ 1+\overline{Z} & -1-l^2k^2 & \dot{\overline{\gamma}} & \overline{W}_{xy}\tau'\\ -b\overline{W}_{xy} & -b\dot{\overline{\gamma}} & -1-l^2k^2 & \overline{Z}\tau'\\ 0 & 0 & k^2/\tilde{\zeta} & -\tilde{D}k^2(1+\xi^2k^2)\end{pmatrix}. \tag{4.5}$$

For convenience, we have changed variables to

$$Z=\frac{a-1}{2}W_{xx}+\frac{1+a}{2}W_{yy} \tag{4.6}$$

and [actually absent from the simplified matrix (4.5)]

$$Y=\frac{a-1}{2}W_{xx}-\frac{1+a}{2}W_{yy}. \tag{4.7}$$

We have also defined renormalized drag

$$\tilde{\zeta}=\frac{(1+a)}{\phi(1-\phi)^2}\zeta \tag{4.8}$$

and diffusion coefficient

$$\tilde{D}=D-\frac{\bar{Z}G'}{\tilde{\zeta}}. \tag{4.9}$$

($\bar{Z}$ is negative so $\tilde{D}>D>0$.) The matrix (4.5) is exact in the uncoupled limit $\zeta\to\infty$. In this limit, therefore, we note that the normal stresses appear only through the linear combination $Z(W_{xx},W_{yy})$, with $Y(W_{xx},W_{yy})$ playing no part. For finite ζ it contains several approximations [72]—most notably neglecting δY—and so underestimates the growth rate of the coupled instability. However, we have checked that the qualitative trends are unaffected. In some places below we further neglect terms of order η. This is valid only for concentrations not too near the critical concentration ϕ_c and shear rates not too far above the lower spinodal, so that $\eta\dot{\gamma}\ll GW_{xy}$. In any case, start-up at higher shear rates is too violent to study experimentally [73].

In order to satisfy the boundary conditions $\partial_y\delta\phi=0$, $\partial_y\delta\underline{\underline{W}}=0$, and $\delta v=0$ (imposed strain rate), only harmonics of the gap size $k_y=n\pi/L$ are allowed. But in order to define the spinodal independently of the system size, we allow arbitrarily small wave vectors.

B. Results: Uncoupled limit

1. Spinodal

In the limit $\zeta\to\infty$ at fixed $D\propto f''/\zeta$, fluctuations in the mechanical variables decouple from those in concentration. Our numerical results for the spinodals in this limit are given by the circles in Fig. 3. The unstable region coincides with that of negative constitutive slope $d\Sigma/d\dot{\gamma}<0$, as expected. It vanishes at a "critical point" $\phi_c\approx0.015$, as in the experiments of Ref. [13].

Analytically, the stability matrix in this limit is exactly

$$\underline{\underline{M}}_{\underline{k}}=\begin{pmatrix}\underline{\underline{M}}_{\mathrm{M}} & - \\ \underline{0} & -Dk^2(1+\xi^2k^2)\end{pmatrix}\begin{matrix}\text{"mechanical"},\\ \delta\phi,\end{matrix} \tag{4.10}$$

in which $\underline{\underline{M}}_{\mathrm{M}}$ is the upper left 3×3 "mechanical" sector of matrix (4.5). (The three elements represented by the dash are nonzero but irrelevant to the eigenvalues since all off-diagonal elements in the bottom row are zero.) Its eigenvalues obey

$$\omega_k^4+a\omega_k^3+b\omega_k^2+c\omega_k+d=0, \tag{4.11}$$

where $d=\mathrm{Det}\,\underline{\underline{M}}_{\underline{k}}$. Since the roots of any such polynomial with real coefficients are either real or complex-conjugate pairs, there are two possibilities for the spinodal. First, the root with the largest real part could be zero, implying the onset of a monotonically growing instability. Alternatively, the root could be one of a pure imaginary pair, implying the onset of growing oscillations. (In the language of dynamical systems' theory, this is the signature of a Hopf bifurcation [74].) For the parameters considered, we have mostly found the first case [75]. Accordingly, our analysis hereafter considers only this first case, for which the spinodal is given by $d=\mathrm{Det}\,\underline{\underline{M}}_{\underline{k}}=0$. Assuming just one unstable eigenvalue (which is the case for the present purposes), $\mathrm{Det}\,\underline{\underline{M}}_{\underline{k}}<0$ in the unstable region, i.e.,

$$D\mathfrak{D}_{\mathrm{M}}>0, \tag{4.12}$$

in which

$$\begin{aligned}\mathfrak{D}_{\mathrm{M}}&\equiv\mathrm{Det}\,\underline{\underline{M}}_{M}\\ &=\frac{k^2}{\eta_s\tau_d}\{-\eta(1+b\bar{\dot{\gamma}}^2)-(1+\bar{Z})+b\bar{W}_{xy}\bar{\dot{\gamma}}\}\\ &=-\left[\frac{k^2}{\eta_s\tau_d}(1+b\bar{\dot{\gamma}}^2)\right]\frac{d\bar{\Sigma}}{d\bar{\dot{\gamma}}}.\end{aligned} \tag{4.13}$$

(We have neglected the interfacial terms l^2k^2 and ξ^2k^2 in calculating the spinodal, because they merely cut off the dispersion relation at short length scales without affecting the sign of the maximum growth rate.) The term in the square brackets of Eq. (4.13) is always positive, so the condition for instability is finally just

$$-D\frac{d\bar{\Sigma}}{d\bar{\dot{\gamma}}}>0. \tag{4.14}$$

From this, we see that CH ϕ demixing can occur if the zero-shear diffusion coefficient is unstable, $D<0$. As noted above, however, in this paper we consider only flow instabilities, and so set $D>0$. The unstable region then is $d\bar{\Sigma}/d\bar{\dot{\gamma}}<0$, as seen numerically: the instability occurs in the upper 3×3 subspace of the matrix (4.10) and so is purely mechanical.

Note that, although the normal stresses [encoded by $Z=Z(W_{xx},W_{yy})$] have apparently canceled from Eq. (4.14), they in fact play a crucial role in the mechanical instability, as follows. The origin of this instability is the positive term $(k^2/\eta_s\tau_d)b\bar{W}_{xy}\bar{\dot{\gamma}}$ in the curly braces of Eq. (4.13). In this term, $-k^2/\eta_s\tau_d$ is the prefactor to δW_{xy} in the $\delta\dot{\gamma}$ equation, and states that a local increase in W_{xy} causes a diffusive decrease in $\dot{\gamma}$. The remaining factor feeds back positively: a

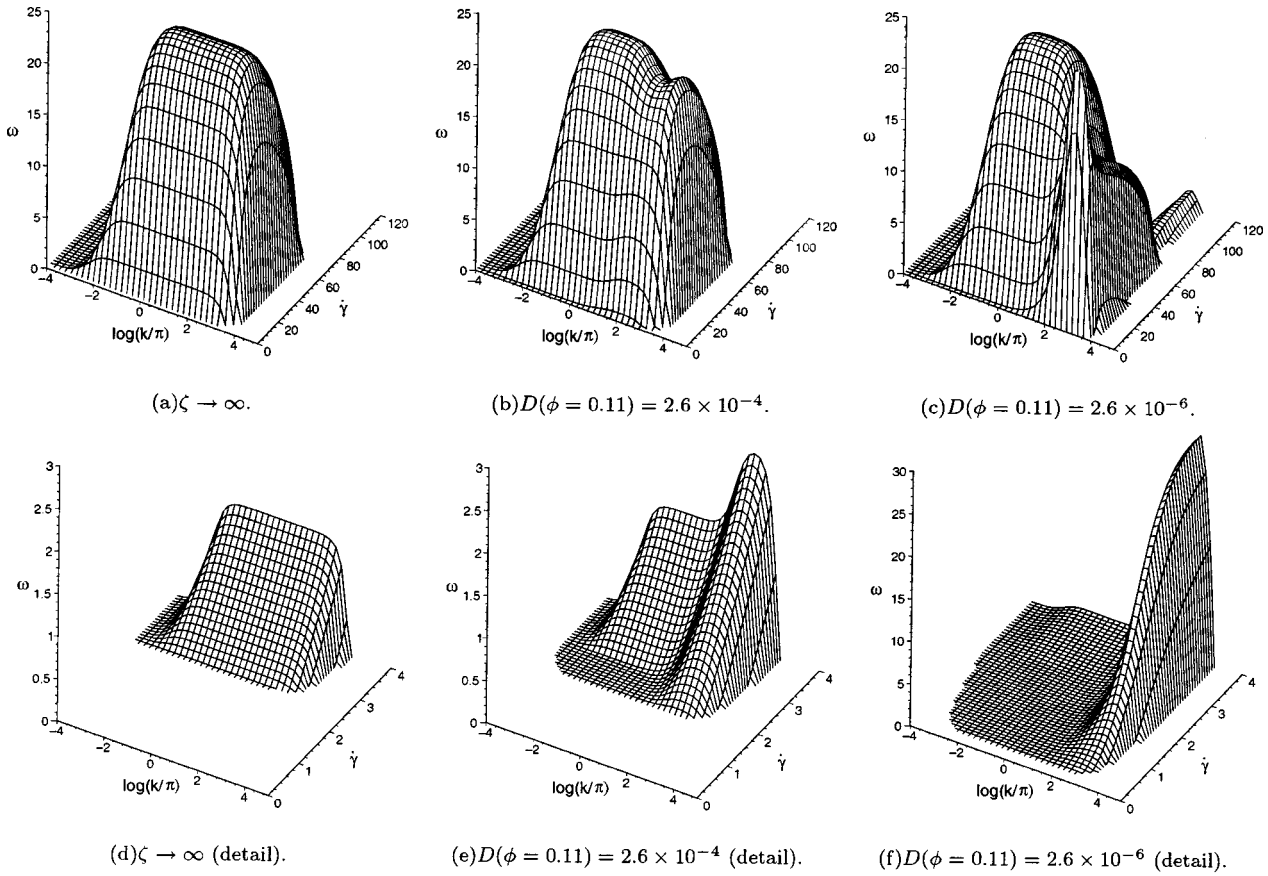

FIG. 4. Positive (unstable) dispersion branch at $\phi=0.11$. (a) and (d) are for the uncoupled model; (b) and (e) are for the coupled model in which all parameters assume the experimental values of Table I (spinodal given by □s in Fig. 3); (c) and (f) are for a coupled model in which $D(\phi)$ is artificially reduced (spinodal given by △s in Fig. 3). For each vertical pair of graphs, the bottom is an enlargement of the top one, at shear rates near the lower spinodal. In each subfigure, the white space defines $(\dot{\gamma},k)$ values for which all dispersion branches are negative.

decrease in $\dot{\gamma}$ causes a constitutive increase in W_{xy}, consistent with the negative slope in the constitutive curve. However, this factor itself describes two mechanisms, each of which involves the normal stress Z. The factor $-b\overline{W}_{xy}$ (prefactoring $\delta\dot{\gamma}$ in the δZ equation) states that the decrease in $\dot{\gamma}$ causes an increase in Z. The remaining factor $\overline{\dot{\gamma}}$ (prefactoring $\delta\dot{\gamma}$ in the δW_{xy} dynamics) states that this increase in Z causes an increase in $\dot{\gamma}$, thereby completing the positive feedback. This role of normal stress was not considered in early studies of mechanical instability [4], although see [76]. Note finally that the *absolute* values of the micellar normal stresses are important, not just the difference $W_{yy}-W_{xx}$: the trace of the *micellar contribution* to the stress tensor is not arbitrary.

Having discussed the spinodal onset of mechanical instability, we now consider the dispersion relations in the unstable regime.

2. Dispersion relation

Before discussing the dispersion relation for fluctuations about an initial state on the intrinsic constitutive curve, we make the following cautionary remark. While the stability analysis of this initial state can correctly define the spinodal *boundary* of instability in sweeps along the flow curve (previous section), it is less useful *inside* the unstable region since one cannot prepare an initial state on the unstable part of the constitutive curve. Indeed, start-up quenches into the unstable region in general go unstable long before the intrinsic constitutive curve can be attained (see Sec. V). However, the main features of the dispersion relation for fluctuations about the unstable constitutive curve do still appear in their time-dependent counterparts of start-up flow. Our motivation for discussing them here is to gain early qualitative insight without the complication of time dependence.

For this pure mechanical instability (with this initial condition) we observe only one positive dispersion branch, shown in Figs. 4(a) for $\phi=0.11$ and 5(a) for $\phi=0.02$. Strictly, only harmonics $k=n\pi$ of the gap size $L\equiv 1$ are allowed. However, we still show $k<\pi$, because for some systems the features of this domain (discussed below) could lie in the allowed region $k\geqslant\pi$. Figure 4(d) contains the same data as Fig. 4(a), but enlarged on shear rates near the lower spinodal: this is the only regime in which banding start-up kinetics have been studied experimentally since they become too violent at higher shear rates [73].

For a given unstable applied shear rate $\overline{\dot{\gamma}}$, the growth rate ω tends to zero as $k\to 0$ and as $k\to\infty$, with a broad plateau

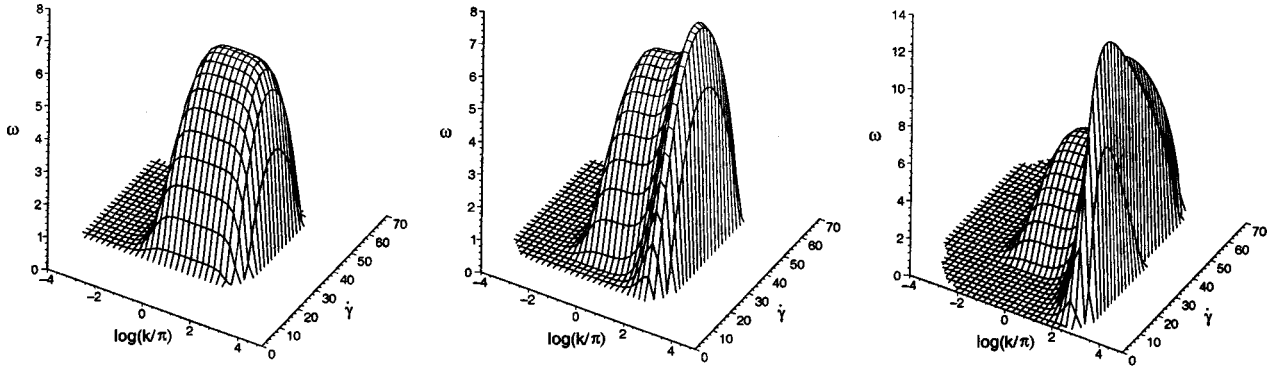

(a)$\zeta \to \infty$. (b)$D(\phi = 0.11) = 2.6 \times 10^{-4}$. (c)$D(\phi = 0.11) = 2.6 \times 10^{-6}$.

FIG. 5. Unstable dispersion branch at $\phi = 0.02$. (a) is for the uncoupled model; (b) is for the coupled model in which at $\phi = 0.11$ all parameters assume the experimental values of Table I (spinodal is given by $\square$s in Fig. 3); (c) is for a coupled model in which $D(\phi = 0.11)$ is artificially reduced (spinodal given by $\triangle$s in Fig. 3). In each subfigure, the white space defines $(\dot{\gamma},k)$ values for which all dispersion branches are negative.

in between. This can be understood via the following analytical results obtained from the characteristic equation of matrix (4.10) and schematized in Fig. 6(a).

(i) *Reynolds regime* $k \to 0$. Here we find

$$\omega_k = -\frac{d\bar{\Sigma}}{d\bar{\dot{\gamma}}}\frac{k^2}{\eta_s \tau_d}. \tag{4.15}$$

This is marked as a dashed line in Fig. 6(a), and agrees well with the numerical data. Here, the instability is limited by the Reynolds rate at which the shear rate (conserved overall) diffuses a distance $O(1/k)$: the micellar stress responds adiabatically in comparison.

(ii) *Nonconserved plateau regime.* At these shorter length scales (but still with $k^2 l^2 \ll 1$) the growth rate is instead limited by the Maxwell time on which the micellar backbone stress evolves (and the Reynolds number is effectively zero). Because micellar stress is nonconserved, the growth rate is independent of k:

$$\omega = \frac{\tilde{\mathfrak{D}}_M}{1+\bar{Z}} = -\frac{1}{(1+\bar{Z})^2}\frac{d\bar{\Sigma}}{d\bar{\dot{\gamma}}} + O(\eta, \tilde{\eta}) \tag{4.16}$$

with

$$\tilde{\mathfrak{D}}_M = \mathfrak{D}_M \frac{\eta_s \tau_d}{k^2}. \tag{4.17}$$

(Recall that $\mathfrak{D}_M \propto k^2$.) The prediction of Eq. (4.16) is marked as a dashed line (also incorporating the interfacial regime, below) in Fig. 6(a).

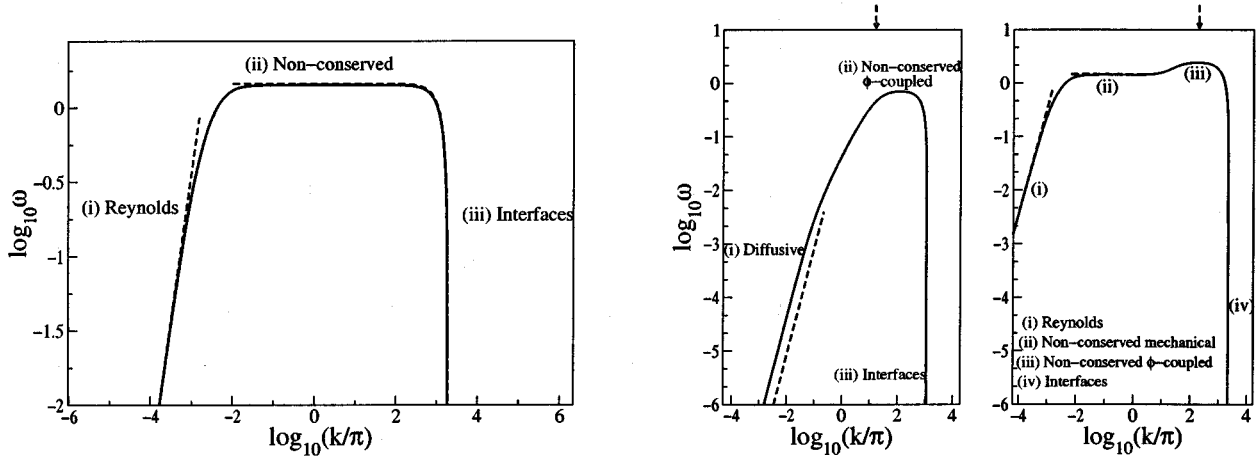

(a)$\phi = 0.11, \zeta \to \infty, \dot{\gamma} = 4.0$. (b)$\phi = 0.11$, $D = 2.6 \times 10^{-4}$, $\dot{\gamma} = 2.55$ (left), $\dot{\gamma} = 4.0$ (right).

FIG. 6. Illustration of the various dispersion regimes discussed in the text: (a) uncoupled mechanical instability, (b) coupled model. (b, left) is for a shear rate that would be stable in the uncoupled limit $\zeta \to \infty$; (b, right) is for a higher shear rate that *is* inside the uncoupled mechanical spinodal. The solid lines are the exact numerical results. The dashed lines are the approximate analytical asymptotes given in Eqs. (4.15), (4.16), and (4.21). The dashed arrows show the approximate k^* of Eq. (4.24).

(iii) *Interfacial cutoff*. The dispersion relation is cut off once $kl=O(1)$ by the reluctance to form interfaces. Here, the growth rate follows from Eq. (4.16) with $\omega \rightarrow \omega + l^2k^2$.

The crossover between the first two regimes occurs at a length scale much greater than the interfacial cutoff, giving a broad intermediate plateau. The maximum in $\omega(k)$ is very shallow and its length scale exceeds the system size for the experimental systems considered here. Therefore fluctuations grow equally quickly at all length scales from any typical system size down to the interface width, and there is no selected length scale, in disagreement with experiment. In the next section, we see that coupling to concentration naturally selects an initial length scale at which inhomogeneity emerges.

Before proceeding, however, we pause to note that several previous authors have considered the mechanical instability of the JS model, without concentration coupling, although few have included the interfacial term required to select the ultimate steady banded state, and which, in this linear analysis, cuts off the dispersion relation at high wave vector. A collection of references can be found in the review [77]. For example, Refs. [7,8] gave a nice analysis of the stability of stationary homogeneous solutions on the intrinsic constitutive curve, at fixed overall stress. They considered the zero Reynolds limit and therefore found no k dependence. In the plane of W_{xy}-Z, they found the lower shear branch to be an attracting node, the upper branch to be a stable focus, and the branch of decreasing stress to be a saddle point. Reference [9] found the condition for instability to be $d\Sigma_{xy}/d\dot{\gamma}<0$, consistent with our analysis. Beyond the JS model, Ref. [5] considered the linear stability of a simple scalar viscoelastic model, without interfacial terms, at zero Reynolds number. Consistent with our analysis, they found no k dependence. Reference [61] studied a scalar viscoelastic model at *finite* Reynolds number, *with* interfacial terms, and did apparently find a selected wave vector. However, there the viscoelastic stress was assumed to respond adiabatically so the intermediate plateau, which in our case eliminates this length scale, was artificially absent.

C. Results: Coupled model

For finite drag, the mechanical instability described above is coupled to fluctuations in concentration $\delta\phi$ via the Helfand-Fredrickson feedback mechanism. As already discussed, the main source of this feedback is the presence of the viscoelastic stress $G(\phi)\underline{\underline{W}}$ in the diffusion equation Eq. (2.16). This causes concentration to diffuse up gradients in W_{yy} at rate $\propto 1/\zeta$. The elastic part of the stress [Eq. (2.13)] then increases in proportion to $G'(\phi)\equiv dG(\phi)/d\phi$, resulting in a positive feedback proportional to G'/ζ, which enhances the mechanical instability. Equation (2.16) actually contains another source of feedback, in the elastic contribution of F_e to the term $\underline{\nabla}(\delta F^e/\delta\phi)$. For completeness we include this in our numerics but neglect it in our analytical work, since it does not affect the qualitative trends at shear rates near the lower spinodal, $\dot{\gamma} > \sim \dot{\gamma}_{c1}$, which are the main ones of interest to us.

1. Spinodal

We now study how this flow-concentration feedback shifts the spinodal onset of instability, so that the lower spinodal now occurs at a shear rate $\dot{\gamma} < \dot{\gamma}_{c1}$. This will have important implications for fast upward stress sweep experiments: ''top'' jumping will now occur *before* the maximum of the underlying flow curve is reached.

Our numerical results are given in Fig. 3. For the experimental model parameter values of Table I the spinodals are shifted only slightly (squares in Fig. 3), so that the instability is still essentially ''mechanical,'' but perturbed by concentration coupling. However, this shift increases dramatically in systems that are near to an underlying CH demixing instability, as illustrated by reducing $D(\phi=0.11)$ at fixed coupling G'/ζ (diamonds and triangles in Fig. 3). For $D \gtrsim 0$, instability sets in at very low shear rates, for which the regime of negative constitutive slope for $\dot{\gamma} > \dot{\gamma}_{c1}$ is essentially irrelevant. At these low shear rates, the instability is essentially CH demixing, triggered by shear. (When D finally goes negative—not shown—demixing must occur even at zero shear.)

On the basis of these results, we classify systems into two basic types.

Type I systems are far from a CH demixing instability. The spinodal is shifted only slightly by concentration coupling.

Type II systems are close to a CH instability ($D \gtrsim 0$). The spinodal is strongly perturbed by concentration coupling.

Correspondingly, we anticipate two types of instability (with a smooth crossover in between).

Type A instabilities, which are essentially mechanical ''shear banding'' (eigenvector mostly in $\delta\dot{\gamma}$, $\delta\underline{\underline{W}}$) but perturbed by coupling to $\delta\phi$. These are expected in all type I systems, and in type II systems for shear rates well above the lower spinodal.

Type B instabilities, which are essentially CH demixing (eigenvector dominated by $\delta\phi$), triggered by flow (SID). These occur in type II systems at shear rates just inside the lower spinodal, see Refs. [36,41,45–48].

This intuition is confirmed by the results given in Sec. V below.

To complement the numerical results of Fig. 3, an approximate analytical condition for instability that qualitatively reproduces the shifts in the lower spinodal [found by setting $\omega_k=0$ in the characteristic equation of the approximate stability matrix (4.5)] is

$$\tilde{D}\mathfrak{D}_M + \frac{1}{\tilde{\zeta}}\mathfrak{D}_F > 0. \tag{4.18}$$

In this inequality, $\mathfrak{D}_M$ is the mechanical determinant already defined in Eq. (4.13); $\mathfrak{D}_F$ is a ''feedback determinant,'' which captures the flow-concentration coupling discussed above:

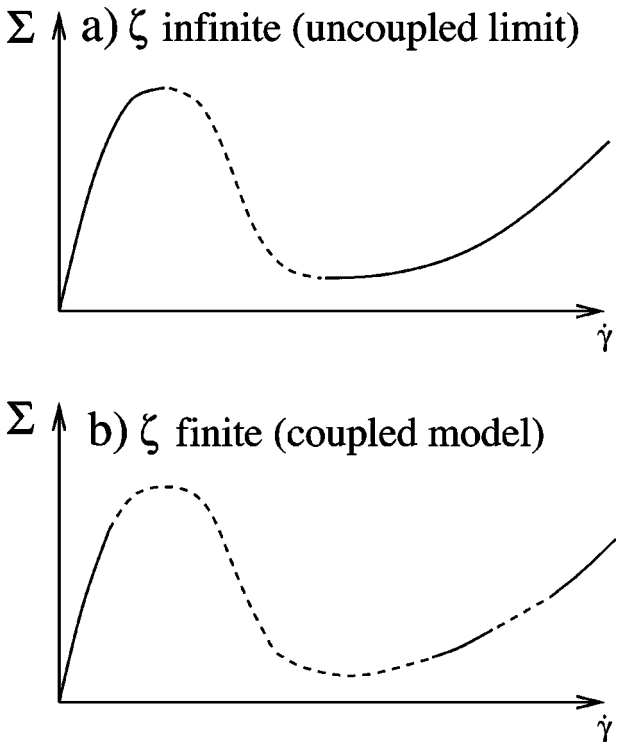

FIG. 7. Sketch of the unstable (dashed) region of a mechanical instability (a) decoupled from or (b) coupled to concentration. As discussed in the text, concentration coupling broadens the region of instability and can sometimes cause a new region of instability to develop in the high shear rate branch (see Fig. 3).

$$\mathfrak{D}_F = \begin{vmatrix} 0 & -\frac{k^2}{\eta_s \tau_d} & -\frac{G' \overline{W}_{xy} k^2}{\eta_s \tau_d} \\ 1+\overline{Z} & -1 & \overline{W}_{xy}\tau' \\ -b\overline{W}_{xy} & -b\dot{\overline{\gamma}} & \overline{Z}\tau' \end{vmatrix} + O(\eta^0, \tilde{\eta}^0)$$

$$= -\frac{k^2}{\eta_s \tau_s} G' \overline{W}_{xy} \{ -b\dot{\gamma}(1+\overline{Z}) - b\overline{W}_{xy} \} + O(\eta^0, \tilde{\eta}^0)$$

$$= -G' \overline{W}_{xy} \left[\frac{k^2}{\eta_s \tau_s} (1 + b\dot{\gamma}^2) \right] \frac{d\overline{Z}}{d\dot{\overline{\gamma}}} + O(\eta^0, \tilde{\eta}^0), \qquad (4.19)$$

where $d\overline{Z}/d\dot{\overline{\gamma}} < 0$. (The terms in τ' cancel each other.) As for the uncoupled model, the interfacial terms have been neglected in locating the spinodal. Our final condition for instability is thus

$$\tilde{D} \frac{d\overline{\Sigma}}{d\dot{\overline{\gamma}}} + \frac{G' \overline{W}_{xy}}{\tilde{\zeta}} \frac{d\overline{Z}}{d\dot{\overline{\gamma}}} < 0, \qquad (4.20)$$

which reduces to the uncoupled condition (4.14) for $\zeta \to \infty$ at fixed D, as required. The size of the second term (which encodes feedback) relative to the "diagonal" product of uncoupled instabilities (first term) is set by $G'/(D\zeta) \sim G'/f''$, i.e., the ratio of the "feedback elasticity" G' to the osmotic elasticity f''. The kinetic coefficient ζ has canceled from this ratio, since the instability occurs adiabatically at the spinodal.

Note finally that a second lobe of instability appears at high shear rates for small values of D. [See Fig. 3 (bottom) and Fig. 7.] However, its existence and location are highly sensitive to the choice of model parameters and to the precise details of model definition: it appears much more readily and extends to much higher shear rates if the Newtonian contribution to the micellar stress is not included. Its eigenvector is overwhelmingly dominated by $\delta\dot{\gamma}$. It is associated with two *complex* eigenvalues with equal positive real parts. We do not study this instability in detail, but return in Sec. VI to discuss its potential implications. The effects of concentration coupling in our model are summarized in Fig. 7.

The enhancement of flow instabilities by concentration coupling was first predicted by the remarkable insight of Schmitt *et al.* [35]. Our Eq. (4.20) corresponds to their Eq. (24), and the flow-concentration feedback mechanism of our model corresponds to their direct assumption of a chemical potential $\mu = \mu(\dot{\gamma})$. However, this is truly equivalent to our approach only if the viscoelastic stress $\underline{\underline{W}}(\dot{\gamma})$ can adjust adiabatically (assumed in Ref. [35]), whereas we find below that the dynamics inside the spinodal *are* dictated by the rate of micellar stress response. (The spinodal is unaffected, since the response here is adiabatic by definition.) Schmitt *et al.* also predicted an instability for negative feedback, but concluded it to be similar in character to a pure mechanical instability in which concentration plays no role. In our model, negative feedback would correspond to $dG/d\phi < 0$; we consider only positive feedback (in the notation of Ref. [35], $C > 0$).

2. Dispersion relation

We now discuss the dispersion relation for fluctuations about a state on the intrinsic constitutive curve when concentration coupling is present. The cautionary remark made in Sec. IV B 2 above for the uncoupled model still applies: one cannot in practice prepare an initial state on the unstable part of this curve.

We have seen in the previous section that concentration coupling enhances the mechanical instability, shifting its lower spinodal to a shear rate $\dot{\gamma} < \dot{\gamma}_{c1}$. We focus mainly, and first, on shear rates just inside this lower spinodal, since this is the only regime in which unstable start-up kinetics are feasibly studied: the instability is too violent at higher shear rates [73]. Comparing the dispersion relation for the pure mechanical instability [Fig. 4(d)] to that for a coupled model of type I [Fig. 4(e)], we see that *concentration coupling enhances the mechanical instability only at short wavelengths, thereby selecting a length scale* k^{*-1}. We discuss this length scale in more detail below. At long wavelengths (small k), the plateau of the uncoupled instability is still apparent (provided $d\Sigma/d\dot{\gamma} < 0$) and unperturbed. For $d\Sigma/d\dot{\gamma} > 0$ this plateau disappears to leave only the diffusive, concentration-coupled bump. The dispersion relation for a system closer to type II (D reduced by a factor 100, at fixed G'/ζ) is shown in Fig. 4(f): the enhancement at long length scales is much

more pronounced, corresponding to the greater spinodal shift (triangles of Fig. 3). However the mechanical plateau (present when $d\Sigma/d\dot{\gamma}<0$) is still unperturbed at long length scales [although indiscernible on the scale of Fig. 4(f)].

The overall dispersion shape is therefore the same in type I and II systems. Its main features can be understood in more detail by analyzing the simplified stability matrix (4.5). We consider two separate cases.

(a) Shear rates *above* the lower spinodal of the *coupled* model but that are still low enough to be mechanically stable in the uncoupled limit [$d\Sigma/d\dot{\gamma}>0$; Fig. 6(b, left)]. Here, we find the following regimes.

(i) *Diffusive regime* $k\to 0$ in which

$$\omega=-\left[\tilde{D}+\frac{1}{\tilde{\zeta}}\frac{\mathfrak{D}_F}{\mathfrak{D}_M}\right]k^2. \tag{4.21}$$

This is marked as a dashed line in Fig. 6(b, left), and slightly underestimates the exact result [72]. The growth rate in this regime is limited by the rate at which matter diffuses a distance $O(1/k)$: momentum diffusion and micellar strain response are adiabatic in comparison. [Note that for larger shear rates for which $d\Sigma/d\dot{\gamma}<0$, discussed in (b) below, Eq. (4.21) gives $\omega<0$, so this branch is absent from the instability; compare Figs. 6(b, left and right).]

(ii) *Nonconserved "plateau" regime.* For larger k, the rate at which the nonconserved micellar strain can respond (even within concentration enhanced dynamics) is the limiting factor; concentration diffusion becomes adiabatic in comparison. If the eventual interfacial cutoff in the dispersion relation once $l^2k^2=O(1)$ or $\xi^2k^2=O(1)$ were absent we would then see a nonconserved k-independent plateau regime in which

$$\omega_{pl}=\frac{\tilde{\mathfrak{D}}_M+\tilde{\mathfrak{D}}_F/\tilde{D}\tilde{\zeta}}{1+\overline{Z}-G'b\overline{W}_{xy}^2/\tilde{D}\tilde{\zeta}}, \tag{4.22}$$

with

$$\tilde{\mathfrak{D}}_i=\mathfrak{D}_i\frac{\eta_s\tau_d}{k^2},\quad i\in F,M. \tag{4.23}$$

(Recall that $\mathfrak{D}_M\propto k^2$ and $\mathfrak{D}_F\propto k^2$.) However, for the systems of interest to us, the low-k crossover to this regime is not well separated from the interfacial cutoff and the plateau is replaced by a rounded maximum at (k^*,ω^*) (thus defined) where $\omega^*<\sim\omega_{pl}$. This maximum selects the length scale k^{*-1} at which structure first emerges, as noted above, and as seen experimentally [32].

(iii) *High k interfacial cutoff.* The dispersion relation is cut off by interfaces once $k^2l^2=O(1)$ or $k^2\xi^2=O(1)$. l and ξ are roughly comparable for the systems of interest to us.

An estimate for the selected wave vector k^* can be obtained by expanding about $\omega\approx\omega_{pl}$ to find

$$k^{*4}\approx\frac{\omega_{pl}}{\tilde{D}\xi^2-\tilde{D}(1+\overline{Z})l^2/\hat{\mathfrak{D}}_M-G'b\overline{W}_{xy}^2l^2/\tilde{\zeta}\hat{\mathfrak{D}}_M}, \tag{4.24}$$

where

$$\hat{\mathfrak{D}}_M=\tilde{\mathfrak{D}}_M-\omega_{pl}(1+\overline{Z})<0. \tag{4.25}$$

This k^* is marked by a dashed arrow in Fig. 6(b), and agrees reasonably with the numerics. As in the conventional CH instability, $k^*\to 0$ at the spinodal (where $\omega^*\to 0$). This is not visible in Figs. 4 and 5, because k^* starts to diminish appreciably only for indiscernibly small ω^* on our scale. Note that Eq. (4.24) does not reproduce the selected wave vector of standard CH theory at zero shear, since phase separation is still affected by the coupling of composition to viscoelastic effects [78] even in this limit.

(b) For higher shear rates that would have been unstable even in the uncoupled limit $d\Sigma/d\dot{\gamma}<0$, the dispersion relation develops a shoulder at small k: see Fig. 6(b, right). As noted above, this is just the large length scale part of the pure mechanical dispersion branch (Sec. IV B), comprising a Reynolds regime and a mechanical nonconserved regime. [See regimes (i) and (ii) in Fig. 6(b, right).] The growth rate here is much faster than diffusion so concentration is absent from the eigenvector. At shorter length scales, concentration *can* keep pace and *is* included. For shear rates that are not too deep inside the unstable region, the dispersion relation then rises to the rounded plateau estimated by Eq. (4.22) [regime (iii) of Fig. 6(b, right)] before finally being cut off by interfaces [regime (iv)]. The maximum at k^* is again estimated by Eq. (4.24) [marked by the dashed arrow in Fig. 6(b, right)].

The preceding analysis captures the qualitative features of the dispersion relations in many regimes. However, some more exotic effects are apparent in Figs. 4(b) and 4(c) for shear rates well above the lower spinodal. For $20\lesssim\dot{\gamma}\lesssim 80$, concentration coupling gives *negative* feedback at short length scales. The origin of this (not included in our above analytical treatment) is that the velocity advecting the micellar backbone strain is not the center of mass velocity $\underline{v}$ (as the above analytical work assumed) but the micellar velocity $\underline{v}_m=\underline{v}+(1-\phi)\underline{v}_{rel}$. A fluctuation δW_{yy} in general causes a fluctuation in ϕ, i.e., in $\underline{v}_{rel}$. When included in the advective term, this feeds back negatively on W_{yy}. At still higher shear rates $\dot{\gamma}>80$ in Fig. 4(c), the dispersion relation has a pronounced ridge corresponding to the high shear rate lobe discussed above and schematized by the right hand dashed line of Fig. 7(b).

3. Fluctuations in the vorticity direction

In the uncoupled limit $\zeta\to\infty$, the mechanical subspace is stable with respect to vorticity fluctuations at all shear rates, while concentration has the usual CH demixing instability for $D<0$. Can coupling influence this instability? In some works [35,47] spinodal shifts have indeed been found. In our model this does not occur, for the following reason. By analogy with the feedback mechanism studied above for $\underline{k}=k\hat{\underline{y}}$, the term in Eq. (2.16) that could participate in positive feedback is $\overline{W}_{zz}G'(\phi)k^2\delta\phi$. In our model (unlike [35,47])

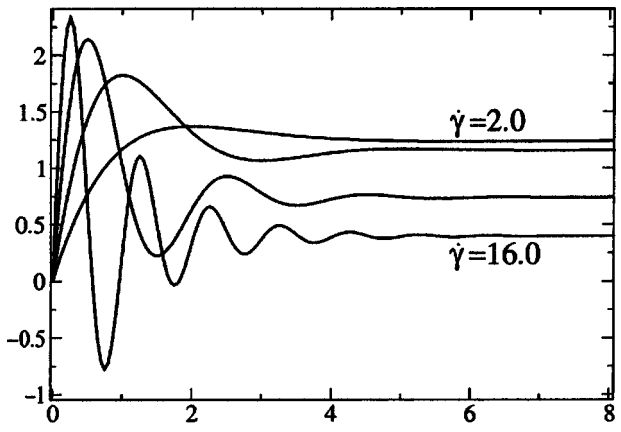

FIG. 8. Homogeneous background micellar strain $\overline{W}_{xy}$ vs t for $\dot{\gamma}=2.0$, 4.0, 8.0, 16.0 (top to bottom at right of plot). For shear rates inside the spinodal, this homogeneous background state can go unstable well before it would have attained time-independence; see text.

$\overline{W}_{zz}=0$ [Eq. (2.22)] so the stability of vorticity fluctuations is unaffected by shear. Accordingly, hereafter we consider only $\underline{k}=k\hat{\underline{y}}$.

V. SHEAR START-UP EXPERIMENT

A. Time dependence and linear analysis

The stability analysis of start-up flow is more involved, because here fluctuations emerge against a background state that itself evolves, deterministically, in time. We first outline these deterministic kinetics (for an idealized noiseless system) before analyzing fluctuations.

1. Deterministic "background" kinetics

At time $t=0$, the rheometer plate at $y=L$ is set in motion with velocity $\overline{\dot{\gamma}}L\hat{\underline{x}}$, giving an instantaneous shear rate profile $\dot{\gamma}(y,0)=\overline{\dot{\gamma}}\delta(y-L)$. On the Reynolds time scale $\tau_{\mathrm{R}}=\rho L^2/\eta\simeq 10^{-3}\tau$, this rapidly homogenizes across the cell such that $\dot{\gamma}(y)=\overline{\dot{\gamma}}$. Then, on the much slower Maxwell time scale τ, the micellar strain starts to evolve homogeneously, according to Eq. (2.17), as

$$W_{xy}(t)=\frac{\overline{\dot{\gamma}}}{1+b\overline{\dot{\gamma}}^2}\{1-e^{-t}[\cos(\sqrt{b}\overline{\dot{\gamma}}t)-\sqrt{b}\overline{\dot{\gamma}}\sin(\sqrt{b}\overline{\dot{\gamma}}t)]\},$$

$$W_{yy}(t)=-\frac{1}{1+a}\frac{b\overline{\dot{\gamma}}^2}{1+b\overline{\dot{\gamma}}^2}\times\left\{1-e^{-t}\left[\cos(\sqrt{b}\overline{\dot{\gamma}}t)+\frac{1}{\sqrt{b}\overline{\dot{\gamma}}}\sin(\sqrt{b}\overline{\dot{\gamma}}t)\right]\right\},$$

$$W_{xx}(t)=\frac{1+a}{a-1}W_{yy}(t),$$

$$W_{zz}(t)=W_{xz}(t)=W_{yz}(t)=0 \tag{5.1}$$

(see Fig. 8). Although these expressions reduce to Eq. (2.22) as $t\to\infty$ (so that the total shear stress would then be on the intrinsic constitutive curve), we show below that in general the flow becomes unstable before this limit is reached.

2. Inhomogeneous fluctuations

In a real system, these homogeneous transients represent only a background state $\underline{\overline{u}}(t)=[\overline{\dot{\gamma}},\underline{\underline{\overline{W}}}(t),\overline{\phi}]$, which is subject to fluctuations induced by noise:

$$\begin{pmatrix}\dot{\gamma}(\underline{r},t)\\ \underline{\underline{W}}(\underline{r},t)\\ \phi(\underline{r},t)\end{pmatrix}=\begin{pmatrix}\overline{\dot{\gamma}}\\ \underline{\underline{\overline{W}}}(t)\\ \overline{\phi}\end{pmatrix}+\sum_{\underline{k}}\begin{pmatrix}\delta\dot{\gamma}(t)\\ \delta\underline{\underline{W}}(t)\\ \delta\phi(t)\end{pmatrix}_{\underline{k}}e^{i\underline{k}\cdot\underline{r}}. \tag{5.2}$$

(As noted above, we are now concerned only with fluctuations $\underline{k}=k\hat{\underline{y}}$.) To investigate the fate of these fluctuations, we linearize (as before) the model's dynamical equations (2.13), (2.14), (2.16), and (2.17) to get a linear stability equation of the form

$$\partial_t\delta\underline{u}_{\underline{k}}(t)=\underline{\underline{M}}_{\underline{k}}(t)\cdot\delta\underline{u}_{\underline{k}}(t)+\underline{\eta}_{\underline{k}}(t), \tag{5.3}$$

where the source term $\underline{\eta}_{\underline{k}}(t)$ arises from the background noise. Equation (5.3) is the counterpart, in start-up, of Eq. (4.3), with the important additional feature that $\underline{\underline{M}}_{\underline{k}}(t)$ is time dependent, via its dependence on the homogeneous background state $\underline{\overline{u}}(t)=[\overline{\dot{\gamma}},\underline{\underline{\overline{W}}}(t),\overline{\phi}]$ as the micellar strain $\underline{\underline{\overline{W}}}(t)$ evolves toward the intrinsic constitutive curve.

Experimentally, the emerging fluctuations $\delta\underline{u}_{\underline{k}}(t)$ are measured in light scattering as the time-dependent static structure factor,

$$\underline{\underline{S}}_{\underline{k}}(t)=\langle\delta\underline{u}_{\underline{k}}(t)\,\delta\underline{u}^{T}_{-\underline{k}}(t)\rangle=\langle\delta\underline{u}_{\underline{k}}(t)\,\delta\underline{u}^{\dagger}_{\underline{k}}(t)\rangle. \tag{5.4}$$

This obeys

$$\partial_t\underline{\underline{S}}_{\underline{k}}(t)=\underline{\underline{M}}_{\underline{k}}(t)\cdot\underline{\underline{S}}_{\underline{k}}(t)+\underline{\underline{S}}_{\underline{k}}(t)\cdot\underline{\underline{M}}^{\dagger}_{\underline{k}}(t)+\underline{\underline{N}}_{\underline{k}}, \tag{5.5}$$

which is exact for the fluctuations considered here. (If $\underline{k}\cdot\hat{\underline{x}}\neq 0$, an extra advective term appears alongside the time derivative.) The noise matrix $\underline{\underline{N}}_{\underline{k}}=\langle\underline{\eta}_{\underline{k}}(t)\,\underline{\eta}^{\dagger}_{-\underline{k}}(t)\rangle$. The solution of Eq. (5.5) is

$$\underline{\underline{S}}_{\underline{k}}(t)=\mathfrak{T}\exp\left[\int_0^t dt''\underline{\underline{M}}_{\underline{k}}(t'')\right]\cdot\underline{\underline{S}}_{\underline{k}}(0)\cdot\exp\left[\int_0^t dt''\underline{\underline{M}}^{\dagger}_{\underline{k}}(t'')\right]+\int_0^t dt'\,\mathfrak{T}\exp\left[\int_{t'}^t dt''\underline{\underline{M}}_{\underline{k}}(t'')\right]\cdot\underline{\underline{N}}_{\underline{k}}(t')\cdot\times\exp\left[\int_{t'}^t dt''\underline{\underline{M}}^{\dagger}_{\underline{k}}(t'')\right], \tag{5.6}$$

where $\underline{\underline{S}}_{\underline{k}}(0)$ is the initial, equilibrium structure factor at the time $t=0$ that shearing is commenced. $\mathfrak{T}$ is a time-ordering

operator that ensures all products of the form $\underline{\underline{\underline{M}}}(t_N)\cdot\underline{\underline{\underline{M}}}(t_{N-1})\cdots\underline{\underline{\underline{M}}}(t_0)$ have $t_N>t_{N-1}>\cdots>t_0$. This is required because the matrix $\underline{\underline{\underline{M}}}_{\underline{k}}$ does not, in general, commute with itself at different times.

Equation (5.6) gives exactly the inhomogeneous fluctuations as they grow (in the unstable regime) out of the homogeneous background state, which is itself evolving toward the intrinsic constitutive curve. It remains valid as long as the fluctuations are small enough that the original linearization of Eq. (5.3) holds, and so predicts just the initial stage of fluctuation growth (our stated aim). To avoid possible confusion, we emphasize that it does *not* require that the evolution of the homogeneous background should be slow compared with the emergence of the fluctuations. This is perhaps contrary to the immediate intuition that, in general, a fluctuation would be swamped as it attempts to emerge, being ''overtaken'' by the growing homogeneous background. Instead, the full state is an independent sum [Eq. (5.2)] of this evolving background ($k=0$) and the (much smaller) emerging fluctuations, which are orthogonal to the base flow ($k>0$).

Direct evaluation of the integral in Eq. (5.6) is very difficult, because the matrix $\underline{\underline{\underline{M}}}_{\underline{k}}=\underline{\underline{\underline{M}}}_{\underline{k}}(\overline{\underline{u}(t)})$ changes over time, and its eigenvectors correspondingly rotate:

$$\omega_{\underline{k},\alpha}(t)\underline{\mathsf{v}}_{\underline{k},\alpha}(t)=\underline{\underline{\underline{M}}}_{\underline{k}}(t)\underline{\mathsf{v}}_{\underline{k},\alpha}(t), \tag{5.7}$$

with explicit time dependence of both $\omega_{\underline{k},\alpha}(t)$ and $\underline{\mathsf{v}}_{\underline{k},\alpha}(t)$. *If* the eigenvectors were (approximately) time independent, i.e., if $\underline{\mathsf{v}}_{\underline{k},\alpha}(t)=\underline{\mathsf{v}}_{\underline{k},\alpha}\ \forall\ t$ over the interval of fluctuation growth, then we could expand in this basis $\underline{\mathsf{v}}_{\underline{k},\alpha}$ to find exactly

$$\begin{aligned}S_{\underline{k},\alpha\beta}(t)=&S_{\underline{k},\alpha\beta}(0)\exp\left[\int_0^t dt''[\omega_{\underline{k},\alpha}(t'')+\omega^*_{\underline{k},\beta}(t'')]\right]\\&+\int_0^t dt'\exp\left[\int_{t'}^t dt''[\omega_{\underline{k},\alpha}(t'')+\omega^*_{\underline{k},\beta}(t'')]\right]\\&\times N_{\underline{k},\alpha\beta}(t')\end{aligned} \tag{5.8}$$

(which, we note, still allows arbitrary values of the rate of fluctuation growth relative to the evolution of the base flow). In reality, however, the eigenvectors rotate in time, so this mode expansion can strictly be performed only in the differential version:

$$\partial_t S_{\underline{k},\alpha\beta}(t)=[\omega_{\underline{k},\alpha}(t)+\omega^*_{\underline{k},\beta}(t)]S_{\underline{k},\alpha\beta}(t)+N_{\underline{k},\alpha\beta}(t). \tag{5.9}$$

Although not the full time integral, this result nonetheless specifies exactly the next small increment in $\underline{\underline{S}}_{\underline{k}}(t)$ at any time. It does *not* require any separation between the rates of fluctuation growth and of evolution of the base flow. It tells us that $\partial_t\underline{\underline{S}}_{\underline{k}}(t)$ is dominated by $S_{\underline{k},\Gamma\Gamma}(t)$, where Γ denotes the most unstable eigenmode $\underline{\mathsf{v}}_{\underline{k},\Gamma}(t)\equiv\underline{\mathsf{v}}_{\underline{k}}(t)$, with the largest $\omega_{\underline{k}}$. In this paper, therefore, we confine ourselves to giving results for this most unstable mode, which determines the main features of the instability. We defer to a future paper [70] calculation of the full start-up structure factor by numerical integration of Eq. (5.5).

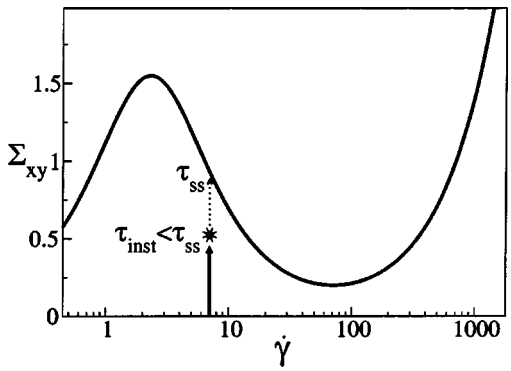

FIG. 9. Cartoon: homogeneous start-up flow going unstable at time $\tau_{\rm inst}$ before it can reach the intrinsic unstable constitutive curve at time $\tau_{\rm ss}$.

In any start-up experiment, then, the micellar strain evolves over a time $\tau_{\rm ss}=O(\tau)$ (thus defined) toward the intrinsic constitutive curve, as described above. The dispersion relation $\omega_{\underline{k},\alpha}(t)$ correspondingly evolves toward the one given by Eq. (4.4) for an initial condition on that flow curve. For a shear rate in the unstable region, then, at least one dispersion branch must go positive at some time $t_0\leqslant\tau_{\rm ss}$ so that the homogeneous transient $[\overline{\dot{\gamma}},\overline{\underline{\underline{W}}}(t),\overline{\phi}$ goes unstable to spatial fluctuations [79]. In most regimes we find only one positive branch [80] and drop the mode subscript α, with the understanding that we mean just this branch, $\omega_{\underline{k}}(t)$. At wave vector $\underline{k}$, the amplitude of the growing fluctuations at a time $t>t_0$ is *approximately* estimated by

$$A(\underline{k},t)\sim\exp\left[\int_{t_0}^t dt'\,\omega_{\underline{k}}(t')\right]. \tag{5.10}$$

[This rough estimate is obtained from a simplified version of Eq. (5.8) and therefore relies on the eigenvectors not rotating too much over the interval $t_0\to t$, i.e., all eigenvector components remaining $O(1)$.] We choose a rough criterion for detectability by light scattering to be $\ln A\simeq 10$. This defines a wave-vector-dependent time scale $\tau_{\rm inst}(\underline{k})$, via

$$\int_{t_0}^{\tau_{\rm inst}(\underline{k})} dt'\,\omega_{\underline{k}}(t')\simeq 10. \tag{5.11}$$

In most regimes, there is a selected wave vector $\underline{k}^*$ at which fluctuations emerge fastest, as the result of a peak in the dispersion relation $\omega_{\underline{k}}(t)$ vs $\underline{k}$. In practice, the peak shifts along the k axis in time, but it is still usually possible to obtain a reasonable estimate of the overall k^*; we justify this claim below. We therefore define the overall time scale of instability to be

$$\tau_{\rm inst}=\tau_{\rm inst}(\underline{k}^*). \tag{5.12}$$

By the time $\tau_{\rm inst}$, then, the system is measurably inhomogeneous and in the nonlinear regime, and our linear calculation terminates. In general, this occurs well before the intrinsic constitutive curve would have been attained, i.e., $\tau_{\rm inst}<\tau_{\rm ss}$ (Fig. 9), so that the instability is determined not by the time-

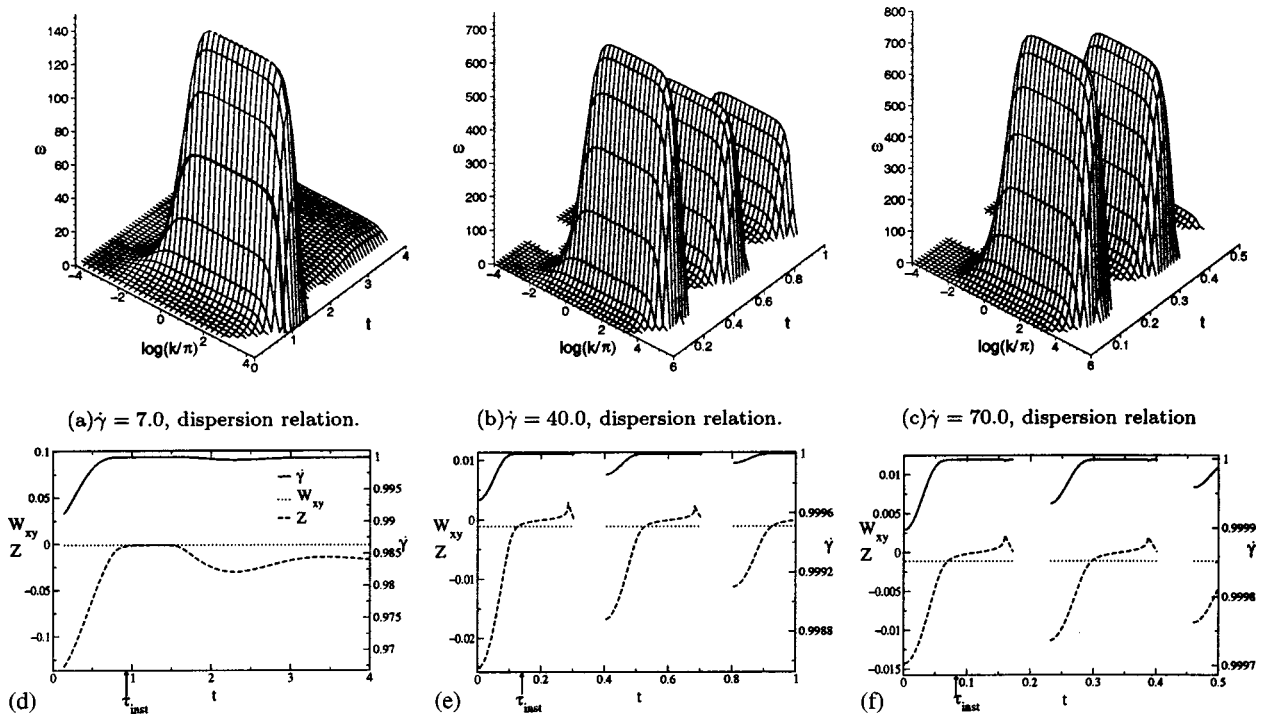

FIG. 10. Type A instabilities in a type I system: time-dependent dispersion relation (top) and eigenvector (bottom) in the uncoupled limit $\zeta \to \infty$ for $\phi = 0.11$. The rheological model parameters all assume the experimental values of Table I. The thick line in (a) and the arrows in (d), (e), (f) denote the time at which the instability becomes measurable. The discontinuities in the first derivative of the eigenvector components result from a crossing of eigenvalues, discussed in the text.

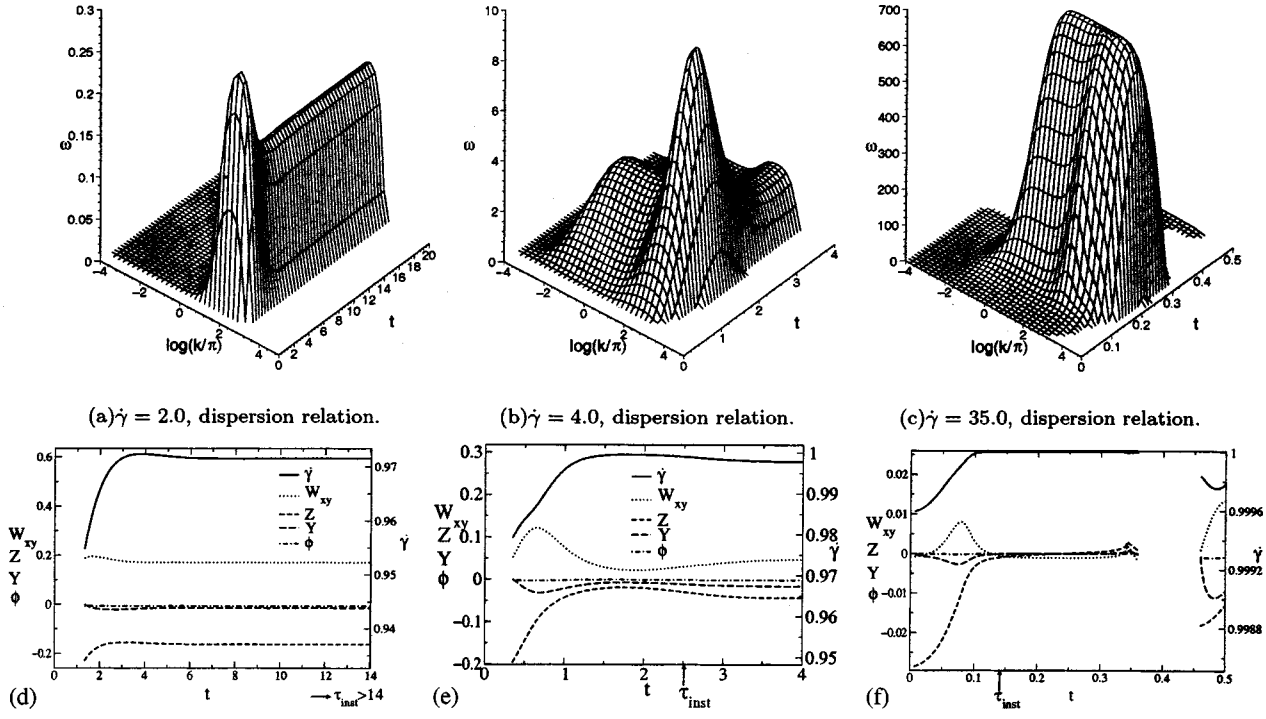

FIG. 11. Type A instabilities in a type I system: time-dependent dispersion relation (top) and eigenvector (bottom) for a coupled model in which all parameters assume the experimental values of Table I. The concentration $\phi = 0.11$. The arrows in (e), (f) show the time at which the instability first becomes measureable [the instability occurs beyond the time window of (d)]. The discontinuities in the first derivative of the eigenvector components result from a crossing of eigenvalues, discussed in the text. The instability time τ_{inst} occurs beyond the displayed time window for $\dot{\gamma} = 2.0$.

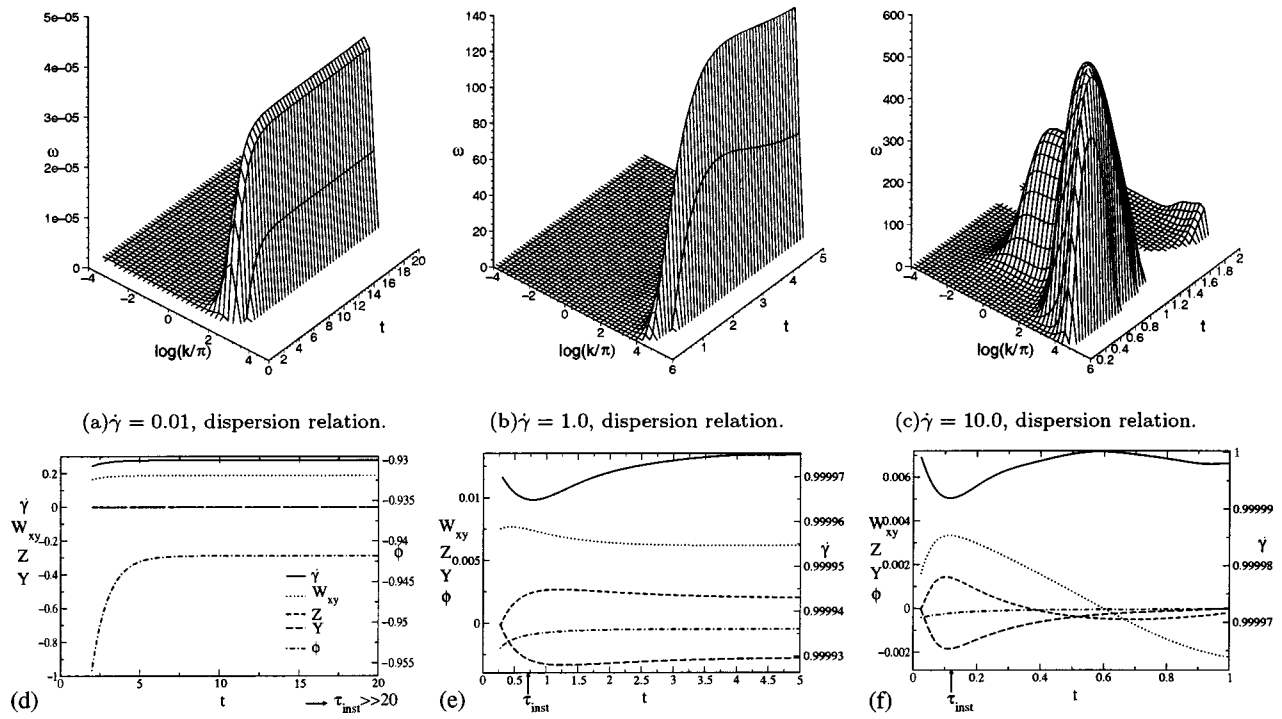

FIG. 12. Type B instabilities (a), (d) and type A instability (b), (c), (e), (f) in a type II system: time-dependent dispersion relation (top) and eigenvector (bottom) for a coupled model in which all parameters assume the experimental values of Table I, *except D*, which is reduced by a factor of 10^5. The concentration $\phi = 0.11$. The arrows in (e), (f) show the time at which the instability first becomes measurable [the instability occurs beyond the time window of (d)].

independent dispersion relations of Sec. IV above, but by their time-dependent counterparts (given below).

Is the unstable intrinsic constitutive curve ever attained before the instability occurs, such that $\tau_{ss} \ll \tau_{inst}$? A *necessary* condition is that the growth rate $\omega_{fc} = \omega_{\underline{k}*}(t = \tau_{ss})$ that would occur once the flow curve were reached (given by the dispersion relations of Sec. IV) obeys [81]

$$\omega_{fc}\tau_{ss} \ll 1. \tag{5.13}$$

This is *not* usually satisfied (recall Figs. 4 and 5) since ω_{fc} is itself set by the Maxwell time τ (with a prefactor set by the slope of the flow curve and by concentration coupling). Nonetheless, the condition (5.13) is satisfied just inside the spinodal, since $\omega_{fc} \to 0$ smoothly at the spinodal. However, this condition is not always *sufficient*. In particular, for shear rates just inside the *upper* spinodal, the homogeneous micellar strain oscillates strongly in start-up. Correspondingly, the growth rate significantly overshoots ω_{fc} (Figs. 10–12 below) and fluctuations still emerge before the intrinsic constitutive curve would be attained. In fact, these oscillations mean that fluctuations can become (temporarily) unstable in start-up, even for shear rates above the upper spinodal (as defined via slow shear rate sweeps). This upper spinodal is therefore not particularly relevant to start-up flows. In any case, shear start-up is generally too violent to study experimentally at such high shear rates [73].

For shear rates just inside the *lower* spinodal, the condition (5.13) is necessary *and* sufficient, and the intrinsic constitutive curve *is* then attained before the instability develops appreciably. Here we can assume, to a good approximation, that the stability matrix changes discontinuously at $t = 0$ from the stable $\underline{\underline{M}}_{\underline{k}}(t = 0)$ (with $\bar{\dot{\gamma}} = \bar{\underline{\underline{W}}} = 0$) to the unstable matrix $\underline{\underline{M}}_{\underline{k}}(t = \infty)$ for a state on the intrinsic constitutive curve. The instability is then, even in start-up, determined by the time-independent dispersion relations of Sec. IV.

We pause to compare our analysis to that of Cahn and Hilliard for a two-component system temperature quenched at time $t = 0$ into the unstable region $\partial\mu(\phi, T)/\partial\phi < 0$, where μ is the chemical potential. A good approximation, invariably made, is that $\mu(\phi)$ changes discontinuously at $t = 0$ from its initial stable state to the final one of negative slope, i.e., that the heat diffuses out instantaneously with respect to the time scale at which fluctuations grow, so that the counterpart of Eq. (5.13) applies. We have just seen that the corresponding assumption for our purposes [the background state $\bar{u}(t)$ instantaneously reaching the intrinsic constitutive curve] is not valid in general.

We now present results for the time-dependent unstable dispersion branch over the time interval $t_0 \to \tau_{inst}$ for several start-up quenches, indicating in each case the selected wave vector k^*. We also give results for the time-dependent eigenvector (at k^*) noting whether separation occurs predominantly in the mechanical variables or in concentration.

B. Start-up dispersion relations and eigenvectors: Uncoupled model

Figure 10 (top) shows the numerically calculated start-up dispersion relation $\omega_{\underline{k}}(t)$ for three different applied shear rates $\dot{\gamma}$ in this uncoupled limit $\zeta \to \infty$. The temporal oscilla-

tions arise from the oscillations in $\underline{\underline{W}}(t)$ toward the intrinsic constitutive curve (Fig. 8). [The time $t \approx 2$ in Fig. 10(a) corresponds to a minimum in $\underline{\underline{W}}(t)$, although the instability actually develops before this, $\tau_{\rm inst} < 2$ [79].] Despite the time dependence, the main features of the time-independent dispersion relation for fluctuations about the intrinsic constitutive curve [Fig. 4(a)] are still apparent: there is a Reynolds regime as $k \to 0$, a nonconserved plateau regime at intermediate k, and interfacial cutoff at large k. As before, then, in this uncoupled limit there is no selected wave vector k^*.

For each start-up, we estimated the time $\tau_{\rm inst}$ at which the instability would become measurable, as governed by criterion (5.11) applied to wave vectors in the plateau regime. It is marked by the thick line in Fig. 10(a) and an arrow in Figs. 10(d)–10(f). For each value of $\dot{\gamma}$ in Fig. 10, we find $\tau_{\rm inst} \ll \tau_{\rm ss}$: instability occurs long before the underlying flow curve would have been attained, as described above.

Figure 10 (bottom) shows the time-dependent eigenvector at wave vector $k^* = \pi$ (chosen arbitrarily since the eigenvector is independent of k in the plateau regime). This is dominated by $\delta\dot{\gamma}$, since $\delta W_{xy} + \eta \delta\dot{\gamma} = 0$ in this zero-Reynolds regime, and η is small. Note also that the normal stress, encoded in δZ, dominates the shear contribution δW_{xy}: consistent with the remarks of Sec. IV B 1, the normal stress plays an important role in this mechanical instability.

The discontinuity in the first derivative of the eigenvector is due to a crossing of two positive eigenvalues: in contrast to the time-independent dispersion relations for fluctuations about the intrinsic constitutive curve, in start-up there is sometimes a second positive dispersion branch, now in the subspace $[ik\delta v_z, W_{xz}, W_{yz}]$. However, this second unstable mode occurs only at high shear rates $\dot{\gamma} \gtrsim 10$, and even then crosses the first only for times well after $\tau_{\rm inst}$: consistent with the claim made above, we never observe mode crossing in the relevant time regime $t \leqslant \tau_{\rm inst}$. This also applies to the coupled model, to which we now turn.

C. Start-up dispersion relations and eigenvectors: Coupled model

We now give start-up results for the coupled model. Denoting the experimental (DLS) value of the diffusion coefficient D (Table I) by $D_{\rm expt}$, Figs. 11 and 12 are for $D = D_{\rm expt}$ (type I system) and $D = 10^{-5} D_{\rm expt}$ (type II system), respectively. The overall features of these dispersion relations are the same as for their time-independent counterparts [Figs. 4 and 6(b)]. In particular, there is, at any time, a well defined peak $k = k_{\rm peak}(t)$. This peak in general shifts along the k axis in time. At $t = t_0$, when $\omega^* = 0$ by definition, we numerically observe that $k_{\rm peak} = 0$. However, $k_{\rm peak}$ very quickly attains a value k^* that is (practically) time independent and well approximated by Eq. (4.24). In this way, the time dependence of $k_{\rm peak}$ occurs only at early times $t > \sim t_0$, for which the growth rate is insignificantly small. We argue, therefore, that we can choose the ultimate $k_{\rm peak} = k^*$ as the representative wave vector for the instability.

The time-dependent eigenvector at this selected wave vector k^* is also shown in Figs. 11 and 12. As noted above, the eigenvector encodes the extent to which separation occurs in each different order parameter. Experimentally, polarized light scattering is sensitive to fluctuations in the micellar strain, while unpolarized light scattering measures fluctuations in the overall micellar concentration.

For type I systems at all (unstable) shear rates [Figs. 11(d), 11(e), and 11(f)], and for type II systems at shear rates that are not too small [Figs. 12(e) and 12(f)], the eigenvector is dominated by the mechanical variables $\delta\dot{\gamma}$ and $\delta\underline{\underline{W}}$ as expected. In this case, the instability can be thought of as mechanical shear banding, perturbed by concentration coupling (type A instability). In contrast, for the type II system at low shear rates [Fig. 12(d)] the eigenvector is dominated by concentration: here the instability is essentially CH demixing, triggered by flow (type B instability). In this way, our model captures a smooth crossover between ''mechanical'' shear banding instabilities and demixing instabilities triggered by flow.

VI. CONCLUSION

In this paper, we have studied early stage kinetics in a unified model of shear banding and shear-induced demixing instabilities, which combines the nonlocal Johnson-Segalman model with a two-fluid approach to concentration fluctuations.

First we calculated the spinodal onset of instability for shear rate sweeps along the underlying constitutive curve. In the absence of coupling between flow and concentration, fluctuations in the mechanical variables (shear rate and stress) are unstable only when the intrinsic constitutive curve has negative slope, as expected. Coupling to concentration enhances this instability via the feedback mechanism of Helfand and Fredrickson, broadening the region of instability. In rapid upward stress sweep experiments, therefore, ''top'' jumping should in fact occur *before* the maximum in the intrinsic constitutive curve is reached. This enhancement increases with proximity to an underlying (zero-shear) CH demixing instability. Accordingly, we classify systems into two types. Type I systems are far from a CH instability, and the mechanical instability is only slightly perturbed by concentration coupling. Closer to a CH instability (type II systems), instability can set in at very low shear rates.

We then calculated the initial structure that emerges after a shear start-up quench into the unstable regime. An important result is that a length scale is selected for this structure only if the mechanical shear banding instability is coupled to concentration. We expect this to be a generic feature of shear banding models.

The eigenvector at this length scale encodes the physical nature of the instability. In type I systems, and type II systems at high shear rates, it is dominated by strain rate and stress. The instability is therefore essentially mechanical shear banding (a type A instability), triggered primarily by the negatively sloping constitutive curve. In type II systems at low shear rates, the eigenvector is dominated by concentration, so we essentially have a shear-induced onset of the nearby thermodynamic fluid-fluid demixing instability (type B), i.e., shear-induced demixing. This crossover is measur-

able experimentally: unpolarized static light scattering measures concentration fluctuations, while polarized scattering couples to the micellar strain.

This unification of mechanical instabilities and shear-induced thermodynamic instabilities is an important finding, since they are often considered as separate phenomena [82]. In this work we have demonstrated a smooth crossover between a shear-induced perturbation of an equilibrium thermodynamic instability, governed by a free energy $F_o(\phi)$ (whose unstable mode is concentration), and a flow-induced instability whose unstable mode is a combination of the structural variables of the strain rate and various components of the micellar strain tensor $\underline{\underline{W}}$. In this case, the flow-induced instability is due to the nonlinear coupling of flow to $\underline{\underline{W}}$.

An analogous example is the relation of the shear banding in semidilute wormlike micelles to the shear-induced isotropic-to-nematic (*I*-*N*) transition in more concentrated systems [20,22,83,84]. Theoretically, the *I*-*N* transition is usually captured via an orientational free energy $F^e(\underline{\underline{Q}})$ in terms of the local orientation tensor $\underline{\underline{Q}}$ [11,12]. Upon coupling the *I*-*N* transition to flow, the equilibrium unstable mode of orientation couples to strain rate so that the unstable mode is now a linear combination of the strain rate and components of $\underline{\underline{Q}}$; and the unstable region is also (usually) associated with the classical hallmark of mechanical instability, i.e., a negatively sloping flow curve $d\Sigma_{xy}/d\dot{\gamma}<0$. Hence, although the physical origins of the instabilities in the type I semidilute (non-nematic) and more concentrated (perturbed *I*-*N*) wormlike micelles are different [in the former case due to the nonlinear coupling of flow to $\underline{\underline{W}}$ and in the latter due to the nonlinear free energy $F^e(\underline{\underline{Q}})$], the signature of the instability is the same in practice; i.e., an unstable flow curve in which the strain rate is coupled to a nonconserved structural tensor (respectively $\underline{\underline{W}}$ and $\underline{\underline{Q}}$).

Finally, in type II systems, we found that a lobe of instability develops at high shear rates, with the character of a Hopf bifurcation [74]. This could clearly have dramatic consequences for any putative coexistence of low shear and high shear bands, since the high shear band could itself be unstable. Indeed, the high shear band is often seen to fluctuate strongly [85], or to break into smaller bands [63]. However, in our model this high shear instability is highly sensitive to choice of model parameters and could be an unrealistic feature.

Our study was confined to fluctuations in the flow gradient direction and to the qualitative features of the instability that can be gleaned from the time-dependent dispersion relations and eigenvectors. In future work, we will present numerical results for the time-dependent unstable static structure factor in start-up, for fluctuations in the entire flow vs flow gradient plane [70]. We also calculate flow phase diagrams for the steady shear banded state [58].

Note added. Recently, Yuan and Jupp numerically studied a similar model of concentration-coupled shear banding.

ACKNOWLEDGMENTS

We thank Paul Callaghan, Ron Larson, Sandra Lerouge, and Tom McLeish for interesting discussions and Grant No. EPSRC GR/N 11735 for financial support; this work was supported in part by the National Science Foundation under Grant No. PHY99-07949.

[1] M.E. Cates, J. Phys. Chem. **94**, 371 (1990).
[2] N.A. Spenley and M.E. Cates, Macromolecules **27**, 3850 (1994).
[3] N.A. Spenley, M.E. Cates, and T.C.B. McLeish, Phys. Rev. Lett. **71**, 939 (1993).
[4] J. Yerushalmi, S. Katz, and R. Shinnar, Chem. Eng. Sci. **25**, 1891 (1970).
[5] N.A. Spenley, X.F. Yuan, and M.E. Cates, J. Phys. II **6**, 551 (1996).
[6] P.D. Olmsted, O. Radulescu, and C.-Y.D. Lu, J. Rheol. **44**, 257 (2000).
[7] D.S. Malkus, J.S. Nohel, and B.J. Plohr, J. Comput. Phys. **87**, 464 (1990).
[8] D.S. Malkus, J.S. Nohel, and B.J. Plohr, SIAM (Soc. Ind. Appl. Math.) J. Appl. Math. **51**, 899 (1991).
[9] R.W. Kolkka, D.S. Malkus, M.G. Hansen, G.R. Ierley, and R.A. Worthing, J. Non-Newtonian Fluid Mech. **29**, 303 (1988).
[10] C.-Y.D. Lu, P.D. Olmsted, and R.C. Ball, Phys. Rev. Lett. **84**, 642 (2000).
[11] P.D. Olmsted and C.-Y.D. Lu, Phys. Rev. E **56**, 55 (1997).
[12] P.D. Olmsted and P.M. Goldbart, Phys. Rev. A **46**, 4966 (1992).
[13] J.F. Berret, D.C. Roux, and G. Porte, J. Phys. II **4**, 1261 (1994).
[14] P.T. Callaghan, M.E. Cates, C.J. Rofe, and J.B.A.F. Smeulders, J. Phys. II **6**, 375 (1996).
[15] C. Grand, J. Arrault, and M.E. Cates, J. Phys. II **7**, 1071 (1997).
[16] R.W. Mair and P.T. Callaghan, Europhys. Lett. **36**, 719 (1996).
[17] R.W. Mair and P.T. Callaghan, Europhys. Lett. **65**, 241 (1996).
[18] M.M. Britton and P.T. Callaghan, Phys. Rev. Lett. **78**, 4930 (1997).
[19] J.F. Berret, D.C. Roux, G. Porte, and P. Lindner, Europhys. Lett. **25**, 521 (1994).
[20] V. Schmitt, F. Lequeux, A. Pousse, and D. Roux, Langmuir **10**, 955 (1994).
[21] E. Cappelaere, J.F. Berret, J.P. Decruppe, R. Cressely, and P. Lindner, Phys. Rev. E **56**, 1869 (1997).
[22] J.F. Berret, D.C. Roux, and P. Lindner, Eur. Phys. J. B **5**, 67 (1998).
[23] H. Rehage and H. Hoffmann, Mol. Phys. **74**, 933 (1991).
[24] J.P. Decruppe, R. Cressely, R. Makhloufi, and E. Cappelaere, Colloid Polym. Sci. **273**, 346 (1995).
[25] R. Makhloufi, J.P. Decruppe, A. Aitali, and R. Cressely, Europhys. Lett. **32**, 253 (1995).
[26] J.P. Decruppe, E. Cappelaere, and R. Cressely, J. Phys. II **7**, 257 (1997).
[27] J.F. Berret, G. Porte, and J.P. Decruppe, Phys. Rev. E **55**, 1668 (1997).
[28] E. Fischer and P.T. Callaghan, Phys. Rev. E **64**, 011501 (2001).
[29] E. Fischer and P.T. Callaghan, Europhys. Lett. **50**, 803 (2000).

[30] J.F. Berret, Langmuir **13**, 2227 (1997).
[31] S. Lerouge, J.P. Decruppe, and C. Humbert, Phys. Rev. Lett. **81**, 5457 (1998).
[32] J.P. Decruppe, S. Lerouge, and J.F. Berret, Phys. Rev. E **63**, 022501 (2001).
[33] S. Lerouge, J.P. Decruppe, and J.F. Berret, Langmuir **16**, 6464 (2000).
[34] J.F. Berret and G. Porte, Phys. Rev. E **60**, 4268 (1999).
[35] V. Schmitt, C.M. Marques, and F. Lequeux, Phys. Rev. E **52**, 4009 (1995).
[36] X.L. Wu, D.J. Pine, and P.K. Dixon, Phys. Rev. Lett. **66**, 2408 (1991).
[37] H. Gerard, J.S. Higgins, and N. Clarke, Macromolecules **32**, 5411 (1999).
[38] E. Wheeler, P. Izu, and G.G. Fuller, Rheol. Acta **35**, 139 (1996).
[39] I.A. Kadoma and J.W. van Egmond, Langmuir **13**, 4551 (1997).
[40] M. Johnson and D. Segalman, J. Non-Newtonian Fluid Mech. **2**, 255 (1977).
[41] F. Brochard and P.-G. deGennes, Macromolecules **10**, 1157 (1977).
[42] S.T. Milner, Phys. Rev. Lett. **66**, 1477 (1991).
[43] P.-G. deGennes, Macromolecules **9**, 587 (1976).
[44] F. Brochard, J. Phys. (Paris) **44**, 39 (1983).
[45] E. Helfand and G.H. Fredrickson, Phys. Rev. Lett. **62**, 2468 (1989).
[46] M. Doi and A. Onuki, J. Phys. II **2**, 1631 (1992).
[47] S.T. Milner, Phys. Rev. E **48**, 3674 (1993).
[48] N. Clarke and T.C.B. McLeish, Phys. Rev. E **57**, R3731 (1998).
[49] A.N. Beris and V.G. Mavrantzas, J. Rheol. **38**, 1235 (1994).
[50] T. Sun, A.C. Balazs, and D. Jasnow, Phys. Rev. E **55**, R6344 (1997).
[51] H. Tanaka, Phys. Rev. Lett. **76**, 787 (1996).
[52] A. Onuki, R. Yamamoto, and T. Taniguchi, J. Phys. II **7**, 295 (1997).
[53] J.L. Goveas and G.H. Fredrickson, J. Rheol. **43**, 1261 (1999).
[54] S.M. Fielding and P.D. Olmsted, Phys. Rev. Lett. **90**, 224501 (2003).
[55] P.G. deGennes, *Scaling Concepts in Polymer Physics* (Cornell University Press, Ithaca, NY, 1975).
[56] The densities typically differ by only about 1%; no observable settling occurs in these systems over a time scale of several months. Even if the densities were different, this would affect only the inertial terms on the LHS of Eq. (2.13), which turn out to affect the instability only at irrelevant length scales (longer than any typical rheometer gap).
[57] We have neglected inertia in $\underline{v}_{\rm rel}$ since it is small compared with the drag force $\zeta \underline{v}_{\rm rel}$. The criterion for this when considering a fluctuation of rate ω and wave vector k about a state of uniform shear rate $\dot{\gamma}$ is $\max[\rho\omega,\rho\dot{\gamma}] \ll \max[\eta k^2,\zeta]$.
[58] S.M. Fielding and P.D. Olmsted, Eur. Phys. J. E **11**, 65 (2003).
[59] X.-F. Yuan and L. Jupp, Europhys. Lett. **60**, 691 (2002).
[60] X.F. Yuan, Europhys. Lett. **46**, 542 (1999).
[61] J.K.G. Dhont, Phys. Rev. E **60**, 4534 (1999).
[62] Equations (2.20) and (2.21) together ensure zero concentration flux at the boundary, even under shear.
[63] S. Lerouge, Ph.D. thesis, University of Metz, 2000.
[64] S.J. Candau, E. Hirsch, and R. Zana, J. Colloid Interface Sci. **105**, 521 (1985).
[65] O. Radulescu and P.D. Olmsted, J. Non-Newtonian Fluid Mech. **91**, 141 (2000).
[66] O. Radulescu and P.D. Olmsted, Rheol. Acta **38**, 606 (1999).
[67] Before rescaling, $\overline{\dot{\gamma}}$, $\overline{\underline{W}}$, and $\overline{\phi}$ had dimensions $[T^{-1}]$, [1], and [1]. Correspondingly, the size and direction of the vector $\underline{u}$ would have been different in different units, and any vector operations must be applied with caution.
[68] A. Onuki, Phys. Rev. Lett. **62**, 2472 (1989).
[69] N.A. Spenley, X.F. Yuan, and M.E. Cates, J. Phys. II **6**, 551 (1996).
[70] S.M. Fielding and P.D. Olmsted (unpublished).
[71] In *start-up* at high shear rates, $\mathfrak{S}_2$ can become unstable; however, it is always less unstable than $\mathfrak{S}_1$ in the relevant time window; see Sec. V.
[72] Matrix (4.5) neglects δY, which amounts to assuming that the velocity convecting the micellar strain is $\underline{v}=\phi \underline{v}_{\rm m}+(1-\phi)\underline{v}_{\rm s}$ and not $\underline{v}_{\rm m}$. It also neglects the positive feedback between flow and concentration involving the derivative $dF^{\rm e}/d\phi$ of the *elastic contribution* to the free energy in Eq. (2.16).
[73] S. Lerouge (private communication).
[74] P. Glendinning, *Stability, Instability and Chaos* (Cambridge University Press, Cambridge, England, 1994).
[75] In the *coupled* model, an oscillatory instability can occur at very high shear rates, as discussed in Sec. IV C 1.
[76] T.C.B. McLeish, J. Polym. Sci., Part B: Polym. Phys. **25**, 2253 (1987).
[77] M. Renardy, J. Non-Newtonian Fluid Mech. **90**, 243 (2000).
[78] A. Onuki and T. Taniguchi, J. Chem. Phys. **106**, 5761 (1997).
[79] For a linear system [Eqn. (5.3)] the *strict* definition of instability, that fluctuations $\delta \underline{u}_{\underline{k}}(t)$ diverge as $t\to\infty$, cannot be determined merely by analyzing the largest eigenvalue $\omega_{\underline{k}}(t)$ for finite times. Indeed, if $\omega_{\underline{k}}$ (transiently) oscillates between $\omega_{\underline{k}}>0$ and $\omega_{\underline{k}}<0$ [Fig. 10(a)], fluctuations that grow while $\omega_{\underline{k}}>0$ might later decay when $\omega_{\underline{k}}<0$ again. However, we adopt the pragmatic definition that start-up becomes unstable at $t=t_0$ if fluctuations grow sufficiently over $t_0\to\tau_{\rm inst}$ to become measurable by scattering (finite amplitude). Whether they later decay when $\omega_{\underline{k}}<0$ again is not revealed by a linear calculation. In any case, for any $\overline{\dot{\gamma}}$ inside the spinodal, $\omega_{\underline{k}}(t\to\infty)>0$ so that the system is always strictly unstable as $t\to\infty$.
[80] There are rare cases of multiple positive branches but never, for any regime investigated, in the relevant window of time $t<\tau_{\rm inst}$.
[81] For start-up flows governed by two well separated time scales τ_1 and τ_2 with $\tau_1 \gg \tau_2$, rather than the single time scale τ of our model, the intrinsic flow curve can be attained for times $\tau_{ss}\simeq\tau_1$ that satisfy $\omega_{\rm fc}\tau_{ss}\simeq 1$, hence violating the condition of Eq. (5.13).
[82] G. Porte, J.F. Berret, and J.L. Harden, J. Phys. II **7**, 459 (1997).
[83] J.F. Berret, D.C. Roux, G. Porte, and P. Lindner, Europhys. Lett. **25**, 521 (1994).
[84] T.A.J. Lenstra, Z. Dogic, and J.K.G. Dhont, J. Chem. Phys. **114**, 10 151 (2001).
[85] M.M. Britton and P.T. Callaghan, Eur. Phys. J. B **7**, 237 (1999).